

Hydrodynamic instability and coalescence in trains of emulsion drops or gas bubbles moving through a narrow capillary

Krassimir D. Danov, Dimitrina S. Valkovska, and Peter A. Kralchevsky *

Laboratory of Chemical Physics and Engineering, Faculty of Chemistry, University of Sofia, 1 James Bourchier Avenue, 1164 Sofia, Bulgaria

Received 28 November 2002; accepted 4 June 2003

Abstract

We investigate the effect of surfactant on the hydrodynamic stability of a thin liquid film formed between two emulsion drops or gas bubbles, which are moving along a narrow capillary. A ganglion (deformed drop or bubble in a pore) is covered by an adsorption monolayer of surfactant. Due to the hydrodynamic viscous friction, the surfactant is dragged from the front part of a moving ganglion toward its rear part. Consequently, the front and rear parts are, respectively, depleted and enriched in adsorbed surfactant. When such two ganglia move one after another, surfactant molecules desorb from the rear part of the first ganglion and are transferred by diffusion, across the intermediate liquid film, to the front part of the second ganglion. This leads to the appearance of a diffusion-driven hydrodynamic instability, which may cause coalescence of the two neighboring drops or bubbles. The coalescence occurs through a dimple-like perturbation in the film thickness, which is due to a local lowering in the pressure caused by a faster circulation of the liquid inside the film, which in turn is engendered by the accelerated surfactant diffusion across the thinner parts of the film. The developed theory predicts the critical distance between the two ganglia, which corresponds to the onset of coalescence, and its dependence on the radius of the capillary channel, velocity of motion, surfactant concentration and type of the operative surface forces. The results can be useful for a better understanding and quantitative description of the processes accompanying the flow of emulsions and foams through porous media.

© 2003 Elsevier Inc. All rights reserved.

Keywords: Coalescence of drops/bubbles in membrane pores; Filtration of emulsions; Foams in porous media; Instability of thin liquid films; Interfacial mass transport; Membrane emulsification

1. Introduction

The motion of emulsion drops or foam bubbles through cylindrical capillaries and porous media play an important role in processes such as enhanced oil recovery and aquifer remediation [1–5], as well as in membrane emulsification [6,7] and emulsion filtration [8–12]. Sometimes, the transport of drops/bubbles along the pores leads to their splitting to smaller fluid particles [6,13]. In other cases, the collisions of the drops/bubbles in channels lead to their coalescence and to the formation of larger particles [9,14]. The knowledge about the two-phase flow in porous media can be used for the experimental modeling and computer simulation of the respective processes [15,16].

The shape of a drop or bubble moving along a capillary tube, the variation of the applied pressure, and the thick-

ness of the liquid film intervening between the solid wall and the fluid particle, have been investigated in a number of theoretical and experimental studies [13,17–28]. In particular, Fairbrother and Stubbs [17] and Bretherton [18] showed that the thickness of the film between a bubble and the capillary wall is related to the capillary radius and the capillary number. Chen [21], Schwartz et al. [22], and Ratulowski and Chang [24] further examined the bubble-wall film thickness. Experiments with trains of bubbles have been carried out by Hirasaki and Lawson [20] and by Ratulowski and Chang [23]. Concerning the film between two neighboring bubbles, the latter authors have calculated the departure of such a film from a plane perpendicular to the capillary wall when a train of bubbles is in motion [23]. Joye et al. [29] examined the asymmetric thinning of the film between two bubbles and derived a criterion for the transition from asymmetric to symmetric regime of film drainage.

An important role is played by the surfactant, which is adsorbed at the surfaces of the drops/bubbles and stabilizes the respective emulsions and foams [29–33]. Ginley and

* Corresponding author.

E-mail address: pk@lcppe.uni-sofia.bg (P.A. Kralchevsky).

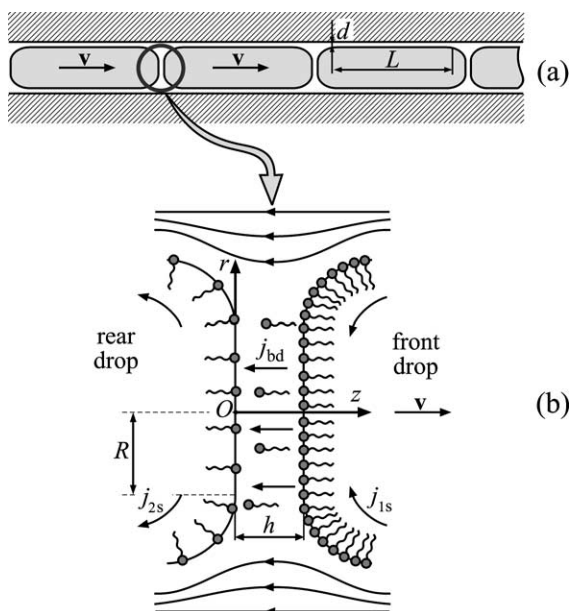


Fig. 1. (a) A train of drops (or bubbles) moving with a constant velocity v along a cylindrical tube; L is the length of the cylindrical film of thickness d intervening between the drop (bubble) and the wall. (b) Sketch of the distribution of surfactant molecules; j_{1s} and j_{2s} are the fluxes of surfactant along the surfaces of the front and rear drop; j_{bd} is the bulk diffusion flux of surfactant across the film (of radius R) separating the two drops (bubbles).

Radke [34] examined the influence of soluble surfactants on the flow of *long* bubbles through a cylindrical capillary. Park [35] described theoretically the effect of surfactants on the motion of a *finite* bubble in a capillary. In particular, it was established [35] that due to the viscous friction, adsorbed surfactant is accumulated at the rear end of the bubble/drop, whereas its front surface is depleted of surfactant (Fig. 1). The respective pattern of fluid motion, accompanied with a surface-tension gradient, to some extent resembles the process of thermocapillary migration [36,37].

In the present paper, we make the next step by considering a train of bubbles/drops, which is moving steadily along a cylindrical capillary. In such a case, one may expect that surfactant molecules (i) desorb from the rear end of the front drop, (ii) cross the gap between the two drops by diffusion, and (iii) adsorb at the front surface of the second drop. As shown in Ref. [38], such a pattern of surfactant transfer across a liquid film gives rise to an instability, which leads to film rupturing and coalescence of the two neighboring drops/bubbles. Our aim in this paper is to investigate theoretically the conditions for the appearance of a stability–instability transition driven by a diffusion transfer of surfactant between neighboring drops/bubbles.

The paper is structured as follows. In Section 2, we present the physical background of the investigated process and identify the factors which govern the difference between the surfactant adsorptions at the front and rear surface of a fluid particle moving along a capillary tube. Section 3 describes the stationary contact region (liquid film) between two neighboring fluid particles. In Section 4, we apply a

linear instability analysis and derive a full set of equations which describe the perturbations of the basic physical parameters. In Section 5, we deduce a characteristic equation determining the value of the “critical” distance between two fluid particles, which corresponds to the stability–instability transition. Finally, in Section 6, we present numerical results and discussion about the influence of various factors (such as the velocity of drop/bubble motion, the radius of the capillary channel, the surfactant concentration, and the action of surface forces) on the stability–instability transition.

2. Physical background

As a rule, the surfaces of the drops in an emulsion, or the bubbles in a foam, are covered by adsorption monolayers of surfactant molecules, which stabilize the respective dispersion. For the sake of brevity, following Ref. [1] we will call “ganglion” a deformed emulsion drop or gas bubble in a pore. As mentioned above, when such a ganglion is moving through a narrow capillary (Fig. 1), the viscous friction in the liquid film, intervening between the drop/bubble and the inner capillary’s wall, influences the surface density (adsorption), Γ , of the surfactant molecules in the adsorbed monolayer. Roughly speaking, in the front part of the ganglion, the surface density decreases with $\delta\Gamma$, whereas in the rear part it increases with $\delta\Gamma$ (a more detailed description is given in Section 3).

To estimate $\delta\Gamma$, let us consider the liquid film between the ganglion and the solid wall. As demonstrated in Refs. [25,35], this wetting film is somewhat thicker in its front part and thinner in its rear part. Here, for the sake of simplicity, we denote by d the average thickness of the wetting film, that is the mean distance between the ganglion surface and the capillary wall. Under steady-state conditions, the stress balance at the ganglion surface reads [39]

$$\frac{\partial\sigma}{\partial z} = \frac{\eta}{d}v_0, \quad (1)$$

where σ is the respective interfacial tension; η is the viscosity of the continuous (film) phase; the z -coordinate is directed along the axis of the capillary (Fig. 1); v_0 is the velocity of the ganglion surface relative to the capillary wall. In the case of a liquid drop (rather than a bubble), Eq. (1) contains an additional term, accounting for the viscous friction inside the drop; however, this term scales with $d/R_c \ll 1$ (R_c is the inner radius of the capillary), and can be omitted. The left-hand side of Eq. (1) can be transformed as

$$\frac{\partial\sigma}{\partial z} = \frac{\partial\sigma}{\partial\Gamma} \frac{\partial\Gamma}{\partial z} = -E_G \frac{\partial \ln \Gamma}{\partial z}, \quad (2)$$

where Γ denotes surfactant adsorption and

$$E_G = -\Gamma \frac{\partial\sigma}{\partial\Gamma} \quad (3)$$

is the surface dilatational (Gibbs) elasticity of the surfactant adsorption monolayer. Combining Eqs. (1) and (2), and in-

tegrating, we get

$$2\delta\Gamma \equiv \Gamma_1 - \Gamma_2 \approx \Gamma_1 \left[1 - \exp\left(-\frac{\eta v_0}{E_G d} L\right) \right], \quad (4)$$

where Γ_1 and Γ_2 are the values of the surfactant adsorption at the right and left surfaces of the film between two drops (see Fig. 1b); L is the length of the wetting film along the capillary axis (Fig. 1a). Taking typical parameter values, $\eta = 1$ mPa s, $L = 10$ μm , $v_0 = 1$ mm/s, $E_G = 10$ mN/m, and $d = 100$ nm, we obtain

$$\frac{\eta v_0 L}{E_G d} = 10^{-2}. \quad (5)$$

When $\eta v_0 L / (E_G d)$ is a small parameter, Eq. (4) can be linearized and we get

$$\delta\Gamma \approx \Gamma_e \frac{\eta v_0 L}{2E_G d}, \quad (6)$$

where Γ_e is the undisturbed (equilibrium) value of the surfactant adsorption at the surface of the fluid particle. Equation (6) shows the dependence of $\delta\Gamma$ on the basic physical parameters.

Now, let us focus our attention at the film (gap) between two neighboring drops/bubbles in the train. As noted earlier, the difference between the surfactant concentrations at the two surfaces of this film gives rise to a diffusion transport of surfactant from the right film surface to the left one (Fig. 1b). For that reason, in the film zone, $\delta\Gamma$ becomes dependent on the radial coordinate, r . This dependence, and the related hydrodynamic fluxes, are considered in the next section.

3. The film between two drops (bubbles)

3.1. The basic (nonperturbed) state of the film

We consider a plane-parallel film of constant thickness, h , and radius, R , situated between two ganglia (drops or bubbles) in the train (Fig. 1b). As before, we will use a cylindrical coordinate system Orz , whose origin is placed in the center of the left film surface (Fig. 1b). The left and right film surfaces correspond to $z = 0$ and $z = h$, respectively. Typically, the film radius, R , is large compared to the film thickness, h . In addition, we assume that the motion of the train of ganglia is slow enough to ensure a small value of the Reynolds number. Therefore, we can use the lubrication approximation to solve the hydrodynamic problem. In this approximation, the pressure p in the continuous phase depends only on the radial coordinate, r , and the time, t : $p = p(r, t)$. Then the Navier–Stokes and continuity equations can be expressed in the form [30,39]

$$\frac{\partial p}{\partial r} = \eta \frac{\partial^2 v_r}{\partial z^2}, \quad (7)$$

$$\frac{1}{r} \frac{\partial}{\partial r} (r v_r) + \frac{\partial v_z}{\partial z} = 0, \quad (8)$$

where v_r and v_z are the velocity components along the respective axes. A double integration of Eq. (7) yields

$$v_r = \frac{z}{2\eta} (z - h) \frac{\partial p}{\partial r} + \frac{z}{h} u_1 + \left(1 - \frac{z}{h}\right) u_2, \quad (9)$$

where u_1 and u_2 are the values of v_r , respectively, at the right and left film surfaces. Hereafter, we will use the indices 1 and 2 to denote quantities related, respectively, to the right and left film surfaces (Fig. 1b). Under steady-state conditions, the distance between the two drops does not change, and consequently

$$v_z|_{z=h} = v_z|_{z=0} = 0. \quad (10)$$

Next, we substitute Eq. (9) into the continuity equation (8), integrate with respect to z , and apply Eq. (10); the result reads

$$\frac{h^2}{6\eta} \frac{\partial p}{\partial r} = u_1 + u_2. \quad (11)$$

3.2. Coupling of diffusion and convection

In the case of drops, we assume that the surfactant is soluble only in the continuous (film) phase, but not in the drop phase. Moreover, we assume that the surfactant is nonionic, and its bulk concentration is below the critical micelle concentration. The “bulk” diffusion problem, which describes the distribution of surfactant molecules in the film interior, will be solved under the following assumptions [32,33,40]: (i) the Peclet number is small, and consequently, the convective terms in the diffusion equation are negligible; (ii) the deviations from equilibrium of the surfactant adsorption Γ are small, see Eqs. (5) and (6); and (iii) the adsorption occurs under diffusion control. As demonstrated in Appendix A, under these assumptions, the surfactant concentration, $c(r, z)$, is a linear function of z ,

$$c(z, r) = c_{2s} + (c_{1s} - c_{2s}) \frac{z}{h}, \quad (12)$$

where $c_{1s}(r) \equiv c(r, z = h)$ and $c_{2s}(r) \equiv c(r, z = 0)$ are the subsurface concentrations at the right and left film surfaces. In accordance with the assumption for small deviations from equilibrium, we present the surfactant concentration and adsorptions at the two film surfaces,

$$c = c_e + \delta c, \\ \Gamma_1 = \Gamma_e + \delta\Gamma(r), \quad \Gamma_2 = \Gamma_e - \delta\Gamma(r), \quad (13)$$

where the subscript “e” denotes the equilibrium values of the respective quantities and δ symbolizes a small increment. The fact that the deviations of adsorption from equilibrium at the two film surfaces have the same magnitude, but the opposite signs, stems from the presumption for a steady-state regime of drop/bubble motion. Under such regime, the incoming flux of surfactant at the right film surface must be equal to the outgoing flux at the left film surface. In other words, $j_{1s} = -j_{2s}$ at $r = R$, see Fig. 1b and Appendix A for

the proof. Having in mind that $c_{1s} = c_e + \delta c_s$, $c_{2s} = c_e - \delta c_s$, and $\delta\Gamma = h_a \delta c_s$, where δc_s is the increment of the sub-surface concentration and $h_a = (\partial\Gamma/\partial c)_e$ is the so called adsorption length, we bring Eq. (12) into the form

$$c(z, r) = c_e + \frac{\delta\Gamma(r)}{h_a} \left(2\frac{z}{h} - 1\right). \quad (14)$$

Under stationary conditions, the linearized balance of surfactant at the two film surfaces reads [30,40]

$$\frac{1}{r} \frac{\partial}{\partial r} \left[r \left(\Gamma u_1 - D_s \frac{\partial \delta\Gamma}{\partial r} \right) \right] = -D \frac{\partial c}{\partial z} \quad \text{at } z = h, \quad (15)$$

$$\frac{1}{r} \frac{\partial}{\partial r} \left[r \left(\Gamma u_2 + D_s \frac{\partial \delta\Gamma}{\partial r} \right) \right] = D \frac{\partial c}{\partial z} \quad \text{at } z = 0, \quad (16)$$

where D and D_s are the coefficients of bulk and surface diffusion. The boundary condition at the periphery of the right film surface (Fig. 1b) is

$$\Gamma_1 = \Gamma_{\max} \equiv \Gamma_e + \delta\Gamma(R) \quad \text{at } r = R, \quad (17)$$

where, for the sake of an estimate, $\delta\Gamma(R)$ can be identified with $\delta\Gamma$ in Eq. (6). Next, we substitute Eq. (14) into Eqs. (15) and (16), and sum up the latter two equations; thus, we obtain

$$u_1 = -u_2 = -u. \quad (18)$$

The comparison of Eqs. (11) and (18) shows that in the basic (nonperturbed) state we have $\partial p/\partial r = 0$. Then, Eq. (9), expressing the radial component of velocity, reduces to

$$v_r = \left(1 - 2\frac{z}{h}\right)u. \quad (19)$$

To close the system of equations, we have to write the boundary condition for tangential stress balance at the film surfaces [30,40],

$$\eta \frac{\partial v_r}{\partial z} = \frac{\partial \sigma}{\partial r} = -\frac{E_G}{\Gamma_e} \frac{\partial \delta\Gamma}{\partial r} \quad \text{at } z = h, \quad (20)$$

$$-\eta \frac{\partial v_r}{\partial z} = \frac{\partial \sigma}{\partial r} = \frac{E_G}{\Gamma_e} \frac{\partial \delta\Gamma}{\partial r} \quad \text{at } z = 0, \quad (21)$$

where the Gibbs elasticity refers to the equilibrium state; see Eq. (3). In Eqs. (20) and (21), the effect of surface viscosity is neglected, insofar as it is usually very small compared to the effect of surface elasticity [32,41]. Substituting Eq. (19) into Eq. (20) or (21), one deduces

$$u = \frac{hE_G}{2\eta\Gamma_e} \frac{\partial(\delta\Gamma)}{\partial r}. \quad (22)$$

Finally, having in mind that $u_1 = -u_2 = -u$, we substitute Eqs. (14) and (22) into Eq. (15) and obtain a second order differential equation for the deviation, $\delta\Gamma$, of adsorption from equilibrium,

$$\frac{1}{r} \frac{\partial}{\partial r} \left[r \frac{\partial(\delta\Gamma)}{\partial r} \right] - q^2 \delta\Gamma = 0, \quad (23)$$

where

$$q^2 \equiv \frac{4b}{3h^2 + h_s h}. \quad (24)$$

The parameters b and h_s , related the coefficients of bulk and surface diffusion, are defined as follows [31,40]:

$$b = \frac{3D\eta}{h_a E_G}, \quad h_s = \frac{6D_s\eta}{E_G}. \quad (25)$$

The solution of Eq. (23), along with the boundary condition, Eq. (17), reads

$$\delta\Gamma(r) = \frac{\Gamma_{\max} - \Gamma_e}{I_0(qR)} I_0(qr). \quad (26)$$

Equation (26) describes the variation of surfactant adsorption throughout the right-hand side surface of the film (Fig. 1b): $\delta\Gamma$ is maximal at the film periphery, where $\delta\Gamma(R) = \Gamma_{\max} - \Gamma_e$, while it is minimal in the center of the film: $\delta\Gamma(0) = \delta\Gamma(R)/I_0(qR)$. The variation of adsorption through the left-hand side film surface is just the mirror image: the variation $\delta\Gamma$ has to be taken with the negative sign there.

3.3. Estimates and numerical examples

To estimate qR , we use data for the nonionic surfactant Triton X-100 from Ref. [42]. The equilibrium surface tension isotherm, $\sigma = \sigma(c)$, of this surfactant at a dodecane–water interface is fitted by means of the Langmuir model [43],

$$\sigma = \sigma_0 + \Gamma_{\infty} kT \ln \left(1 - \frac{\Gamma}{\Gamma_{\infty}}\right), \quad Kc = \frac{\Gamma}{\Gamma_{\infty} - \Gamma}, \quad (27)$$

where σ_0 is the surface tension of pure water, K is an adsorption parameter and Γ_{∞} is the maximum possible adsorption. The parameters of the model, determined from the best fit, are as follows [42]: $K = 0.132 \text{ m}^3/\mu\text{mol}$ and $\Gamma_{\infty} = 1.75 \mu\text{mol}/\text{m}^2$. In addition, $\eta = 1 \text{ mPa s}$, $D = 2.6 \times 10^{-6} \text{ cm}^2/\text{s}$ [42]; for the sake of our estimate we take $D_s = D$; E_G is computed using Eq. (3).

Figure 2 shows the plot of qR vs c computed with the help of Eqs. (24) and (25) for three values of the film radius: $R = 5, 10, \text{ and } 50 \mu\text{m}$. The used parameter values for Triton X-100 are specified after Eq. (27). One sees that in a wide range of concentrations we have $qR \leq 2$, which means that in this range the Bessel function $I_0(qr)$ can be approximated with a parabola:

$$I_0(qr) \approx 1 + (qr)^2/4, \quad r \leq R. \quad (28)$$

For the instability analysis, presented in Section 5, we will use Eq. (28), which much simplifies the mathematical transformations. In other words, we will work in the range of surfactant concentrations, c , and film radii, R , for which Eq. (28) is valid. In such a case, Eqs. (26) and (22) acquire the forms

$$\delta\Gamma(r) = a_1 + a_2 \frac{r^2}{R^2}, \quad u(r) = \alpha \frac{r}{R}, \quad (29)$$

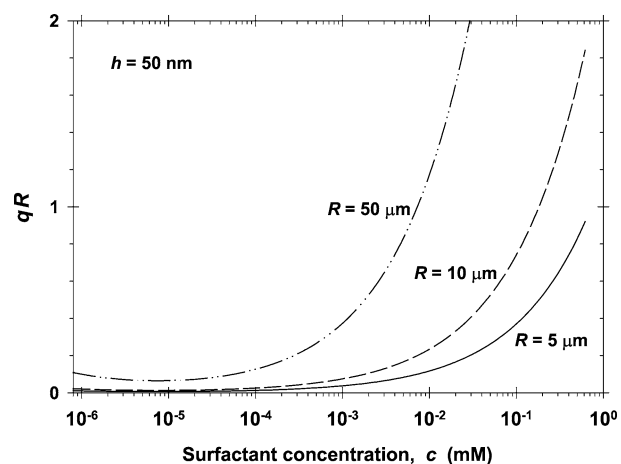


Fig. 2. The argument, qR , of the modified Bessel function, I_0 in Eq. (26), as a function of the surfactant concentration, c , at fixed film thickness, $h = 50$ nm, for three different values of the film radius, R , specified in the figure ($1 \text{ mM} = 0.001 \text{ mol/dm}^3$). The parameter values are estimated for the nonionic surfactant Triton X-100, see the text.

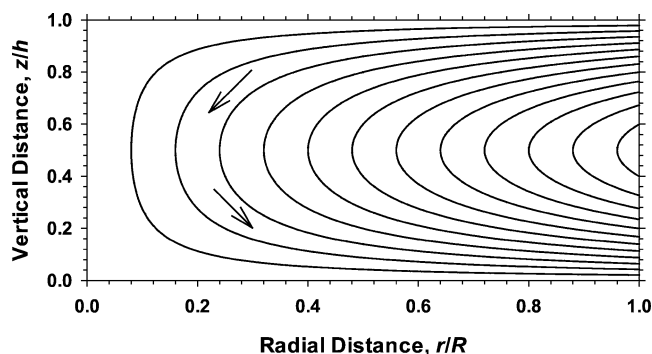


Fig. 3. The streamlines of the flow inside the film between two drops/bubbles (Fig. 1b), calculated with the help of Eqs. (8), (19), and (29). The coordinates $r/R = 0$ and $r/R = 1$, correspond to the film center and periphery, respectively.

$$a_1 = \frac{\delta\Gamma(R)}{1 + (qR/2)^2}, \quad a_2 = \frac{(qR)^2}{4}a_1, \quad (30)$$

$$\alpha = \frac{hE_G a_2}{\eta\Gamma_e R}.$$

Figure 3 illustrates the streamlines of the flow inside the film between two drops/bubbles (Fig. 1b), calculated with the help of Eqs. (8), (19), and (29). As could be expected, at the surface of the front ganglion ($z = h$) the velocity is directed from the periphery ($r = R$) toward the center ($r = 0$), whereas at the surface of the rear ganglion ($z = 0$), the velocity is directed from the center toward the periphery.

Figure 4 shows the variation of the adsorption at the film center, $\delta\Gamma(0)$, scaled with the respective quantity at the film periphery, $\delta\Gamma(R)$. To specify the material parameters, such as Γ_e , E_G , h_a , D , etc., we have used the same set of data for Triton X-100, as for Fig. 2. Figure 4 demonstrates that $\delta\Gamma(0)/\delta\Gamma(R)$ decreases (the nonuniformity of the surfactant interfacial distribution increases) with the rise of film radius and surfactant concentration, and with the decrease

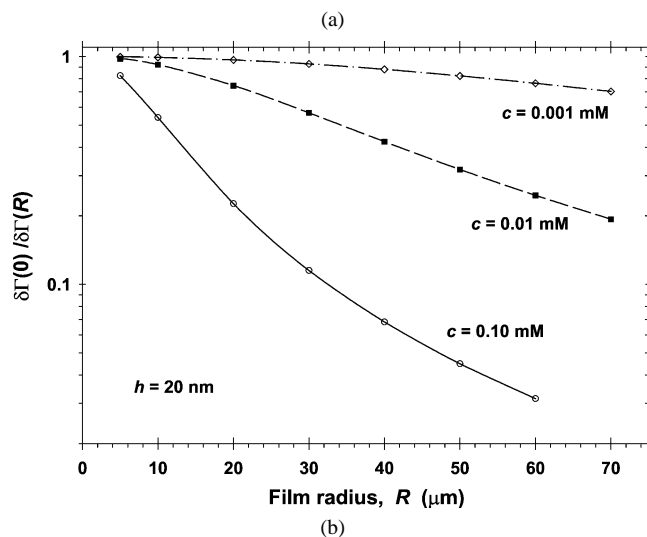
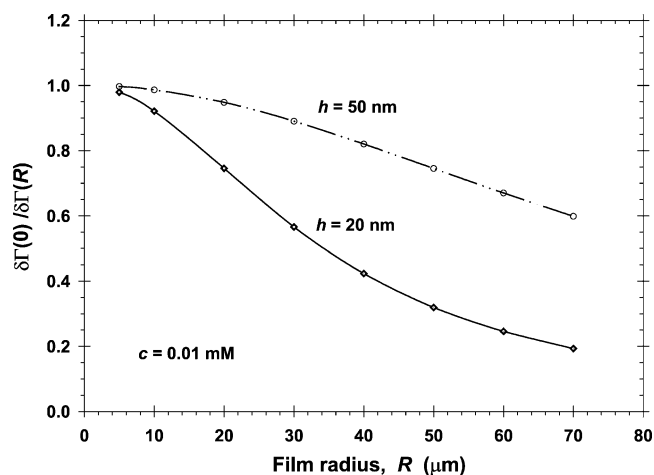


Fig. 4. Adsorption at the film center, $\delta\Gamma(0)$, scaled with the adsorption at the film periphery, $\delta\Gamma(R)$, plotted vs the film radius, R : (a) for constant surfactant (Triton X-100) concentration at two fixed values of the film thickness, h ; (b) for constant $h = 20$ nm at three different fixed surfactant concentrations.

of film thickness. In other words, the adsorption gradient is greater for thinner films with larger radii, at higher surfactant concentrations. For example, at $h = 20$ nm, $c = 0.1$ mM, and $R = 35$ μm , $\delta\Gamma$ in the film center is about 10 times lower than at the film periphery.

4. Perturbations: linear stability analysis

4.1. Connections between the perturbations of various parameters

Due to the inevitable thermal fluctuations or mechanical perturbations, the basic stationary state of the film between two moving ganglia can be disturbed. Depending on the specific conditions (surfactant concentration, film thickness, velocity of motion), the perturbation either could be suppressed, or could spontaneously grow until the film broke

and the two ganglia coalesced. To describe this transition from stability to instability theoretically, we will apply a linear stability analysis.

We present each physical parameter as a sum of its value in the basic state plus a small perturbation, the latter denoted by a tilde:

$$\begin{aligned} v_r &\rightarrow v_r + \tilde{v}_r, & v_z &\rightarrow v_z + \tilde{v}_z, \\ u_1 &\rightarrow -u + \tilde{u}_1, & u_2 &\rightarrow u + \tilde{u}_2, \end{aligned} \quad (31)$$

$$\begin{aligned} h &\rightarrow h + \tilde{h}, & h_1 &\rightarrow h + \tilde{h}_1, \\ h_2 &\rightarrow \tilde{h}_2, & p &\rightarrow p + \tilde{p}, \end{aligned} \quad (32)$$

$$\begin{aligned} c &\rightarrow c + \tilde{c}, & \Gamma_1 &\rightarrow \Gamma_1 + \tilde{\Gamma}_1, \\ \Gamma_2 &\rightarrow \Gamma_2 + \tilde{\Gamma}_2. \end{aligned} \quad (33)$$

The substitution of Eqs. (31)–(33) into the hydrodynamic equations, which represent either stress and mass balances, or kinematic relationships, leads to a full set of equations determining the perturbations of the physical parameters. As before, the subscripts 1 and 2 refer to quantities related to the film surfaces at $z = h$ and $z = 0$, respectively; see Fig. 1b. Here we outline the principles of the theoretical derivations, while the details are given in Appendix B.

In general, we deal with 14 perturbations of physical parameters:

$$\tilde{h}, \tilde{p}, \tilde{u}_1, \tilde{u}_2, \tilde{\Gamma}_1, \tilde{\Gamma}_2, \quad (34)$$

$$\tilde{h}_1, \tilde{h}_2, \tilde{c}|_{z=h}, \tilde{c}|_{z=0}, \tilde{v}_r|_{z=h}, \tilde{v}_r|_{z=0}, \tilde{v}_z|_{z=h}, \tilde{v}_z|_{z=0}. \quad (35)$$

Six equations provide relationships between these perturbations, as follows: the Navier–Stokes equation (7), the continuity equation (8), the two surface mass balance equations, (15) and (16), and the two surface stress balances, Eqs. (20) and (21). We need eight additional equations to close the system. One of them is the geometric relationship

$$\tilde{h} = \tilde{h}_1 - \tilde{h}_2. \quad (36)$$

Other equations are derived as kinematic relationships:

$$u_1 + \tilde{u}_1 \equiv v_r|_{z=h+\tilde{h}_1} = v_r|_{z=h} + \tilde{v}_r|_{z=h} + \frac{\partial v_r}{\partial z} \Big|_{z=h} \tilde{h}_1. \quad (37)$$

Substituting Eqs. (18) and (19) into Eq. (37), we derive

$$\tilde{v}_r|_{z=h} = \tilde{u}_1 + \frac{2u}{h} \tilde{h}_1. \quad (38)$$

The latter equation shows the difference between $\tilde{v}_r|_{z=h}$ and \tilde{u}_1 . Likewise, for the other film surface one can deduce

$$\tilde{v}_r|_{z=0} = \tilde{u}_2 + \frac{2u}{h} \tilde{h}_2. \quad (39)$$

Analogous expressions can be obtained for \tilde{v}_z ,

$$\begin{aligned} v_z|_{z=h+\tilde{h}_1} &= v_z|_{z=h} + \tilde{v}_z|_{z=h} + \frac{\partial v_z}{\partial z} \Big|_{z=h} \tilde{h}_1 \\ &= \tilde{v}_z|_{z=h} + \frac{1}{r} \frac{\partial}{\partial r} (ru) \tilde{h}_1, \end{aligned} \quad (40)$$

where at the last step we have employed Eqs. (8) and (10). On the other hand, we have

$$v_z|_{z=h+\tilde{h}_1} = \frac{\partial \tilde{h}_1}{\partial t} + v_r|_{z=h} \frac{\partial \tilde{h}_1}{\partial r} = \frac{\partial \tilde{h}_1}{\partial t} - u \frac{\partial \tilde{h}_1}{\partial r}. \quad (41)$$

Combining Eqs. (40) and (41) we derive

$$\tilde{v}_z|_{z=h} = \frac{\partial \tilde{h}_1}{\partial t} - \frac{1}{r} \frac{\partial}{\partial r} (ru \tilde{h}_1). \quad (42)$$

Likewise, for the other film surface we obtain

$$\tilde{v}_z|_{z=0} = \frac{\partial \tilde{h}_2}{\partial t} + \frac{1}{r} \frac{\partial}{\partial r} (ru \tilde{h}_2). \quad (43)$$

Two additional equations follow from the normal stress balances at the film surfaces, that is from the respective Laplace equations [38,39],

$$\sigma \nabla^2 h_1 = p_d - p - \Pi(h), \quad (44)$$

$$\sigma \nabla^2 h_2 = p + \Pi(h) - p_d, \quad (45)$$

where p_d is the pressure inside the drops, and p is the pressure in the film. For the basic state of a plane-parallel film, we have $p_d - p = \Pi(h)$. By using Eq. (32) and the relationship $\Pi(h + \tilde{h}) \approx \Pi(h) + \Pi' \tilde{h}$, from Eqs. (44) and (45) we deduce

$$\tilde{p} + \Pi' \tilde{h} + \frac{\sigma}{r} \frac{\partial}{\partial r} \left(r \frac{\partial \tilde{h}_1}{\partial r} \right) = 0, \quad (46)$$

$$\tilde{p} + \Pi' \tilde{h} - \frac{\sigma}{r} \frac{\partial}{\partial r} \left(r \frac{\partial \tilde{h}_2}{\partial r} \right) = 0. \quad (47)$$

In view of Eq. (36), taking the sum and the difference of Eqs. (46) and (47), we get

$$\tilde{p} + \Pi' \tilde{h} + \frac{\sigma}{2r} \frac{\partial}{\partial r} \left(r \frac{\partial \tilde{h}}{\partial r} \right) = 0, \quad (48)$$

$$\tilde{h}_1 = -\tilde{h}_2 = \frac{\tilde{h}}{2}. \quad (49)$$

According to Eq. (49), the normal stress balance implies that the deviations in the two film surfaces from planarity are symmetrical, that is we are dealing with the so-called squeezing (peristaltic) mode of film-surface deformation [44–46]. The bulk diffusion equation,

$$\frac{\partial c}{\partial t} + \mathbf{v} \cdot \nabla c = D \nabla^2 c, \quad (50)$$

provides an additional connection between the perturbations of the physical parameters, see Appendix B. In summary, the eight equations needed to close the system are Eqs. (36), (38), (39), (42), (43), (48), (49), and (50).

4.2. Instability analysis

As we consider fluctuational capillary waves, we will seek the perturbations of the physical parameters in the form [41]

$$\tilde{y} = Y(r) \exp(\omega t), \quad (51)$$

where \tilde{y} can be every of the parameters in Eqs. (34) and (35), $Y(r)$ is the respective amplitude and ω is the *exponent of growth* of the capillary waves. Indeed, for $\omega > 0$ the capillary waves grow until break the liquid film, whereas for $\omega < 0$ the capillary waves decay with time. Therefore, the condition $\omega = 0$ corresponds to the stability–instability transition. Our aim below is to investigate how this transition depends on the physical parameters of the system. Equation (51) implies that in transitional regime ($\omega = 0$) we have

$$\left. \frac{\partial \tilde{y}}{\partial t} \right|_{\omega=0} = 0. \tag{52}$$

In Appendix B it is shown that the perturbations given by Eq. (35) can be eliminated and one arrives at a system of six equations for the remaining six parameters, specified by Eq. (34). In the latter equations, we set the time derivatives equal to zero, in accordance with Eq. (52), to obtain a system determining the *transitional* regime. This system involves Eq. (48) and the following five equations (see Appendix B):

$$\frac{h^2}{6\eta} \frac{\partial \tilde{p}}{\partial r} = \tilde{u}_1 + \tilde{u}_2, \tag{53}$$

$$h\tilde{p} = -\frac{E_G}{\Gamma_e}(\tilde{\Gamma}_1 + \tilde{\Gamma}_2), \tag{54}$$

$$\frac{4u\eta}{h^2}\tilde{h} + \frac{2\eta}{h}(\tilde{u}_1 - \tilde{u}_2) = \frac{E_G}{\Gamma_e} \frac{\partial}{\partial r}(\tilde{\Gamma}_2 - \tilde{\Gamma}_1), \tag{55}$$

$$u(\tilde{\Gamma}_2 - \tilde{\Gamma}_1) + \Gamma_e(\tilde{u}_1 + \tilde{u}_2) - D_s \frac{\partial}{\partial r}(\tilde{\Gamma}_1 + \tilde{\Gamma}_2) = 0, \tag{56}$$

$$\begin{aligned} & \frac{1}{r} \frac{\partial}{\partial r} \left[r \left(u\tilde{\Gamma}_2 + \Gamma_e\tilde{u}_2 - D_s \frac{\partial \tilde{\Gamma}_2}{\partial r} \right) \right] \\ &= \frac{D}{h} \left(\frac{\tilde{\Gamma}_1 - \tilde{\Gamma}_2}{h_a} - 2 \frac{\delta\Gamma}{hh_a} \tilde{h} \right). \end{aligned} \tag{57}$$

When two identical fluid particles (drops, bubbles) approach each other, and the liquid is expelled from the gap between them, at a given stage the hydrodynamic viscous force counterbalances the capillary pressure, and an almost plane-parallel film forms [40,47]. This film continues to thin, remaining nearly planar. For film thickness $h < 50$ – 100 nm, the effect of disjoining pressure, Π , shows up. If the attractive surface force (say the van der Waals interaction) is predominant ($\Pi < 0$), the thinning film loses its stability at a given critical thickness, h_{cr} , the corrugations of the film surfaces grow until the film ruptures; see, e.g., Refs. [48,49]. For foam films (between two bubbles) the critical thickness is typically in the range $h_{cr} = 25$ – 50 nm [49,50]. In contrast, if some repulsive forces (electrostatic, steric, oscillatory–structural) are predominant ($\Pi > 0$), the thinning film reaches an equilibrium thickness, h_{eq} , see, e.g., Refs. [47,51–53]. For example, the equilibrium thickness of a foam film stabilized by an ionic surfactant is $h_{eq} \approx 25$ nm for 0.01 M background ionic strength. The diffusion-driven instability, investigated in the present paper, may lead to film rupturing at considerably greater film thicknesses, say $h > 200$ nm, where the effect of the colloidal surface forces

(disjoining pressure) is completely negligible, see below. For this reason, when a diffusion-driven instability appears, the effect of Π plays a secondary role with respect to the occurrence of the stability–instability transition. Therefore, to simplify our mathematical derivations, below we will restrict our considerations to the case when only van der Waals forces are operative between the film surfaces; in this case [51–53]

$$\Pi' = \frac{A_H}{2\pi h^4}, \tag{58}$$

where A_H is the Hamaker constant. (Up to here we have not specified the expression for Π .) In principle, it is possible to generalize our approach also to the other colloidal surface forces, but as already noted, the major source of instability in the considered system is the surfactant transfer across the film, rather than the surface forces. In some of our computations, to compare numerically the effect of attractive and repulsive surface forces, we formally worked with positive and negative values of A_H , and found that this results only in a slight shift of the boundary between the domains of stable and unstable films, see below.

5. Characteristic equation

The system determining the stability–instability transition, Eqs. (48) and (53)–(57), consists of three algebraic and three differential equations. In Appendix C we show that it is possible to eliminate four of the unknown variables, and to obtain a system of two differential equations,

$$\bar{p} + A\bar{h} + \frac{1}{x} \frac{\partial}{\partial x} \left(x \frac{\partial \bar{h}}{\partial x} \right) = 0, \quad 0 \leq x \leq 1, \tag{59}$$

$$\begin{aligned} & \frac{\partial}{\partial x} \left[x \frac{\partial}{\partial x} \left(\frac{1}{x} \frac{\partial \bar{p}}{\partial x} \right) + N_1 x^2 \bar{h} - N_2 x^2 \bar{p} \right] \\ &= (qR)^2 \frac{\partial \bar{p}}{\partial x} - \left(\frac{4}{(qR)^2} + x^2 \right) N_3 x \bar{h}, \end{aligned} \tag{60}$$

where we have introduced the following dimensionless parameters:

$$\begin{aligned} \bar{p} &\equiv \frac{2R^2}{\sigma h} \tilde{p}, & \bar{h} &\equiv \frac{\tilde{h}}{h}, & x &\equiv \frac{r}{R}, \\ A &\equiv \frac{A_H R^2}{\pi \sigma h^4}, \end{aligned} \tag{61}$$

$$\begin{aligned} N_1 &= \frac{9E_G h (qR)^6 a_1}{4b\sigma(h+h_s)\Gamma_e^2}, & N_2 &= \frac{\sigma h^2 N_1}{4E_G R^2}, \\ N_3 &= \frac{2bR^2}{3h^2} N_1. \end{aligned} \tag{62}$$

In general, the solution of Eqs. (59)–(60) depends on five integration constants. Two of them are determined from natural boundary conditions at the axis of rotational symmetry, $x = 0$; the remaining three constants are to be determined from the boundary conditions at the film periphery.

To demonstrate this, we apply the Frobenius method. Owing to the rotational symmetry, the functions $\bar{h}(x)$ and $\bar{p}(x)$ can be expanded in series including only even powers of x :

$$\bar{h} = \sum_{k=0}^{\infty} H_k x^{2k}, \quad \bar{p} = \sum_{k=0}^{\infty} P_k x^{2k}. \quad (63)$$

To determine the coefficients H_k and P_k , we substitute the expansions, Eq. (63), into Eqs. (59) and (60). After some transformations, we obtain the following relationships between the coefficients H_k and P_k :

$$P_0 = -AH_0 - 4H_1, \quad P_1 = -AH_1 - 16H_2, \quad (64)$$

$$P_2 = \frac{1}{8} \left[N_2 P_0 - N_1 H_0 + (qR)^2 P_1 - \frac{2N_3}{(qR)^2} H_0 \right], \quad (65)$$

$$H_{k+1} = -\frac{1}{4(k+1)^2} (P_k + AH_k), \quad k = 2, 3, \dots, \quad (66)$$

$$P_{k+3} = \frac{1}{4(k+2)(k+3)} \left[N_2 P_{k+1} - N_1 H_{k+1} - \frac{N_3}{k+2} H_k + (qR)^2 P_{k+2} - \frac{2N_3}{(k+2)(qR)^2} H_{k+1} \right], \quad k = 0, 1, \dots \quad (67)$$

The latter result has the following advantages: (i) the recursive relations (64)–(67) provide convenient explicit expressions for all coefficients in the expansions (63); (ii) the recursive relations lead to the fact that H_k and P_k diminish $\propto (k!)^{-2}$, and consequently, the series are well convergent; (iii) the three constants of integration, which remain to be determined from the boundary conditions, are H_0 , H_1 , and H_2 . To find them, we construct three pairs of functions ($j = 1, 2, 3$),

$$F_j(x) = \sum_{k=0}^{\infty} H_{k,j} x^{2k}, \quad G_j(x) = \sum_{k=0}^{\infty} P_{k,j} x^{2k}, \quad (68)$$

where the coefficients $H_{k,j}$ and $P_{k,j}$ are the coefficients H_k and P_k calculated from Eqs. (64)–(67) by setting $(H_0, H_1, H_2) = (1, 0, 0)$, $(0, 1, 0)$, and $(0, 0, 1)$, respectively, for $j = 1, 2$, and 3 . Then, the general solution of Eqs. (59) and (60) can be presented in the form

$$\bar{h} = C_1 F_1(x) + C_2 F_2(x) + C_3 F_3(x), \\ \bar{p} = C_1 G_1(x) + C_2 G_2(x) + C_3 G_3(x), \quad (69)$$

where the constants C_1 , C_2 , and C_3 have to be determined from the boundary conditions at the film periphery. Gumerman and Homsy [54] have found that the results of the instability analysis are not so sensitive to the type of the boundary condition imposed at the periphery of a liquid film. To specify this boundary condition, in our case we will require the perturbations to vanish at the film periphery; that is,

$$\bar{h}|_{x=1} = 0, \quad \left. \frac{\partial \tilde{\Gamma}_1}{\partial r} \right|_{r=R} = \left. \frac{\partial \tilde{\Gamma}_2}{\partial r} \right|_{r=R} = 0. \quad (70)$$

The latter boundary conditions, which are currently used to solve film-instability problems, are related to the fact that

the factors promoting the *growth* of the capillary waves are operative only inside the liquid film [40]. The boundary conditions for the derivatives of $\tilde{\Gamma}_1$ and $\tilde{\Gamma}_2$ in Eq. (70) can be transformed in terms of derivatives of \bar{p} with the help of Eqs. (54) and (C.1), the latter in Appendix C. Thus, Eq. (70) acquires the form

$$\bar{h}|_{x=1} = 0, \quad \left. \frac{\partial \bar{p}}{\partial x} \right|_{x=1} = 0, \quad \left. \frac{\partial^2 \bar{p}}{\partial x^2} \right|_{x=1} = 0, \quad (71)$$

see Appendix C for details. The substitution of Eqs. (69) into (71) gives a system of three linear equations for determining C_1 , C_2 , and C_3 ,

$$\sum_{j=1}^3 a_{ij} C_j = 0, \quad i = 1, 2, 3, \quad (72)$$

where

$$a_{1j} = \sum_{k=0}^{\infty} H_{k,j}, \quad a_{2j} = \sum_{k=0}^{\infty} k P_{k,j}, \\ a_{3j} = \sum_{k=0}^{\infty} k^2 P_{k,j}. \quad (73)$$

Because the linear system (72) is homogeneous, the necessary condition for existence of a nontrivial solution is

$$\det[a_{ij}(h)] = 0. \quad (74)$$

Equation (74) is the sought-for characteristic equation, which determines the value of the film thickness, $h = h_{tr}$, corresponding to the transition from stable to unstable films. Following Refs. [41,49], we call this thickness *transitional*. Note that in Eq. (74) we have a 3×3 determinant, which can be presented by a simple algebraic expression. Equation (73) gives its elements, a_{ij} , as infinite sums of the coefficients $H_{k,j}$ and $P_{k,j}$ which, in their turn, are simply expressed by the recursive formulas (64)–(67), as explained after Eq. (68). Our computations, described in the next section, showed that Eq. (74) has a maximum physical root for h , for all used sets of input parameters. We did not encounter any difficulties related to existence of several roots.

Some remarks about the used mathematical approach are following. The spectral problem, Eqs. (59), (60), (71), and (72), contains differential equations with *variable* coefficients, and for that reason we cannot seek a solution $\propto \exp(\mathbf{k} \cdot \mathbf{r})$, \mathbf{k} is the wave vector, following the conventional approach [41,45]. In such a case, one could apply a *numerical*, finite-differences approach, which is based on a splitting of the interval $0 \leq x \leq 1$ on many subintervals. Say, if we introduce 100 subintervals, we get a system of 100 equations, which has 100 roots. As a result, it is very difficult to identify the physical root corresponding to the stability–instability transition. Alternatively, one can follow an *analytical* approach, which is based on finding of the spectral functions of the problem. Unfortunately, in our case these are not the standard Bessel functions. For that reason,

we found the spectral functions in the form of series expansions, following the Frobenius method, see Eqs. (63)–(67). In fact, this is an exact solution of the problem.

6. Numerical results and discussions

6.1. Principles of the computational procedure

1. The input parameters are the surfactant concentration, c ; the film radius, R ; the adsorption parameters K and Γ_∞ ; the Hamaker constant, A_H ; the bulk viscosity, η , the deviation of adsorption from equilibrium at the film periphery, $\delta\Gamma(R)$, and the surfactant diffusivity, D ; as before, for the surface diffusivity we set $D_s = D$. Note that Eqs. (29) and (30) provide a simple connection between $\delta\Gamma(R)$ and $u(R)$, the latter being the radial surface velocity at the film periphery:

$$u(R) = \frac{hE_G}{\eta\Gamma_e R} \frac{(qR/2)^2}{1 + (qR/2)^2} \delta\Gamma(R). \quad (75)$$

2. With the help of Eqs. (3) and (27), for each given c we calculate the surface tension, σ , the equilibrium adsorption, Γ_e , the adsorption parameter $h_a = (\partial\Gamma/\partial c)_e$, and the Gibbs elasticity, E_G . Next, the parameters b and h_s are determined from Eq. (25).

3. For a tentative value of the film thickness, h , from Eqs. (24) and (30) we calculate the parameters q and a_1 , and then we find N_1 , N_2 , and N_3 from Eq. (62). Further, the coefficients $H_{k,j}$ and $P_{k,j}$ are computed as explained after Eq. (68), and the summation in Eq. (73) is carried out to determine $a_{ij}(h)$.

4. Equation (74), considered as an implicit equation for h , is solved numerically, with the help of the bisection method, and thus the value of the transitional thickness, $h = h_{tr}$, is determined.

6.2. Stability–instability diagrams

In our computations, the values of the parameters K , Γ_∞ , and D were taken for the nonionic surfactant Triton X-100, as specified after Eq. (27). In fact, the procedure described in the previous section allowed us to calculate the transitional value of one among the six parameters, h , $\delta\Gamma(R)$, A_H , R , c , and η , for given values of the remaining five parameters. The numerical results shown in Figs. 5–9 illustrate the influence of various parameters on the stability–instability transition, related to coalescence of neighboring drops (or bubbles) in the train (Fig. 1). Note that the nonperturbed plane-parallel film could be either equilibrium or slowly thinning, see the comments after Eq. (57) above. In the latter case, the stability–instability diagram shows at which transitional thickness, $h = h_{tr}$, the thinning film will lose its stability.

The curves in Fig. 5a show calculated transitional values of the film thickness, $h = h_{tr}$, as a function of $\delta\Gamma(R)$.

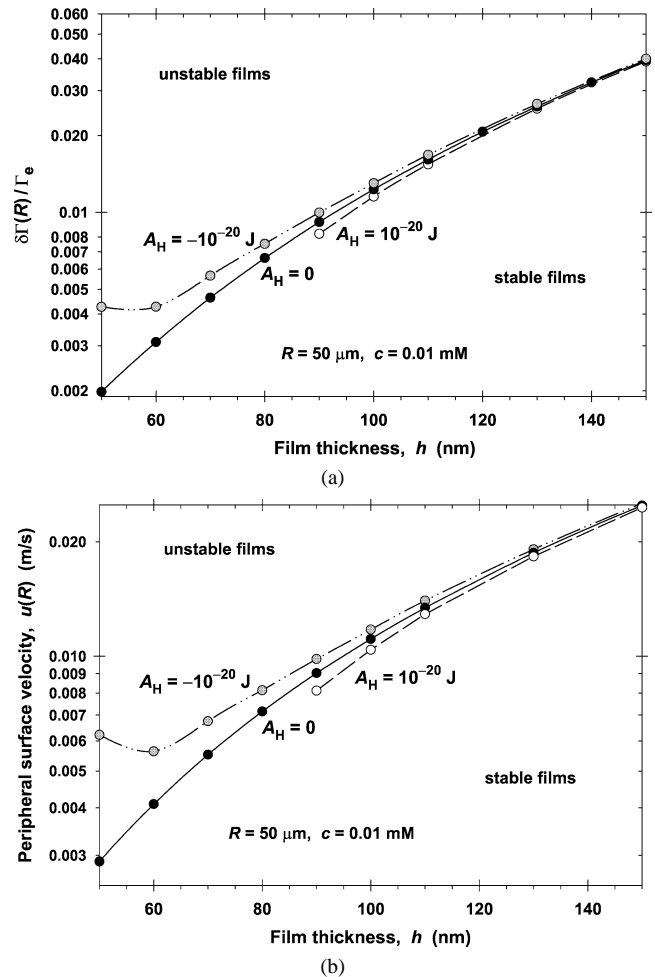


Fig. 5. Stability–instability diagrams calculated for three different fixed values of the Hamaker constant, A_H , denoted in the figure; for all curves $R = 50 \mu\text{m}$, $c = 0.01 \text{ mM}$, and $\eta = 1 \text{ mPa}\cdot\text{s}$. Each curve represents the boundary between the regions of stable and unstable films, where $h = h_{tr}$. (a) Diagram in coordinates $\delta\Gamma(R)/\Gamma_e$ vs h . (b) Diagram in coordinates $u(R)$ vs h ; see Eq. (75).

In addition, Fig. 5b shows the same diagram, but with the peripheral surface velocity, $u(R)$, computed by means of Eq. (75) from the respective $\delta\Gamma(R)$. Each curve, representing the boundary between stable and unstable films/ganglia, corresponds to a given fixed value of the Hamaker constant, A_H . The region of unstable films corresponds to larger $\delta\Gamma(R)$ and $u(R)$, but to smaller film thickness, h (Fig. 5). One sees that the boundary between the stable and unstable films is not so sensitive to A_H . Note that the conventional theory of liquid film breakage due to the growth of capillary waves [49,55], predicts instability only in the case of attractive surface forces, that is, for $A_H > 0$; see Eq. (77) below. Figure 5 demonstrates that in our case instabilities appear also when surface forces are absent ($A_H = 0$) and even when they are repulsive ($A_H < 0$). The weak effect of the colloidal surface forces is not surprising because, in our system, the diffusion transfer of surfactant across the film is the major source of instability. Similar system was investigated in Ref. [38]. The respective physical mechanism of sponta-

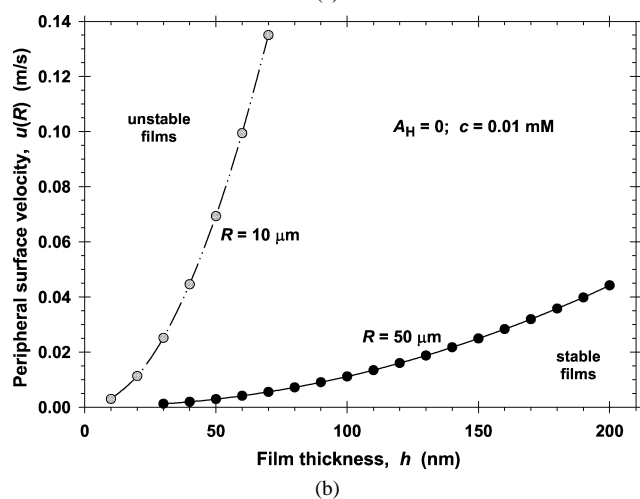
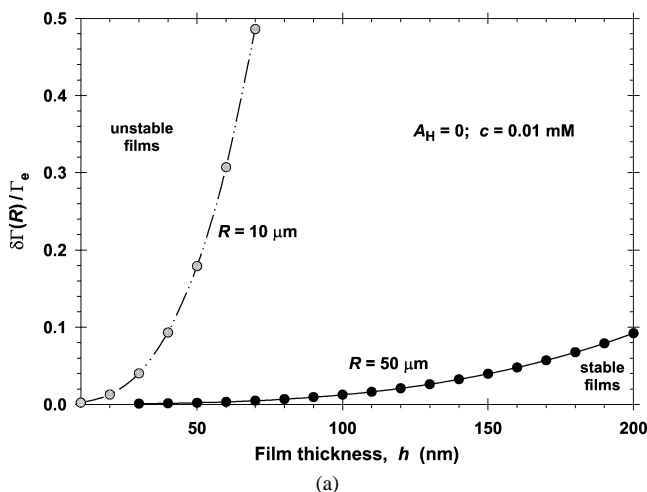


Fig. 6. Stability–instability diagrams calculated for two different fixed values of the film radius, R , denoted in the figure; for all curves $A_H = 0$, $c = 0.01 \text{ mM}$, and $\eta = 1 \text{ mPa s}$. Each curve represents the boundary between the regions of stable and unstable films. (a) Diagram in coordinates $\delta\Gamma(R)/\Gamma_e$ vs h . (b) Diagram in coordinates $u(R)$ vs h .

neous growth of a local perturbational concavity in the liquid film is described in Section 6.3 below.

Figure 6 illustrates the effect of the film radius, R , on the position boundary separating the regions of stable and unstable films. One sees that the stability markedly decreases with the increase of R . This is a result from the higher adsorption gradient for films of larger radii. For $R = 50 \mu\text{m}$, even very thick films ($h = 200 \text{ nm}$) may become unstable due to the diffusion transfer of surfactant across the film.

Additional results for the effect of R are shown in Fig. 7, where the stability diagram is plotted in coordinates $u(R)$ vs R . As it could be expected, the region of unstable films corresponds to the greater values of u and R . The stability of the films (and of the drops/bubbles in Fig. 1) increases with the rise of the thickness, h , of the film between two neighboring drops/bubbles.

The film stability depends also on the viscosity, η , of the continuous (outer) fluid phase because it influences the bulk and surface hydrodynamic fluxes. To elucidate this depen-

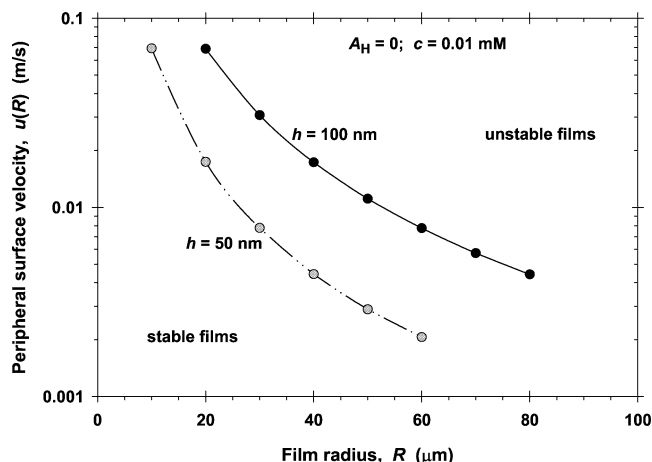


Fig. 7. Stability–instability diagram, $u(R)$ vs R , calculated for two different fixed values of the film thickness, h , denoted in the figure; for all curves $A_H = 0$, $c = 0.01 \text{ mM}$, and $\eta = 1 \text{ mPa s}$. Each curve represents the boundary between the regions of stable and unstable films.

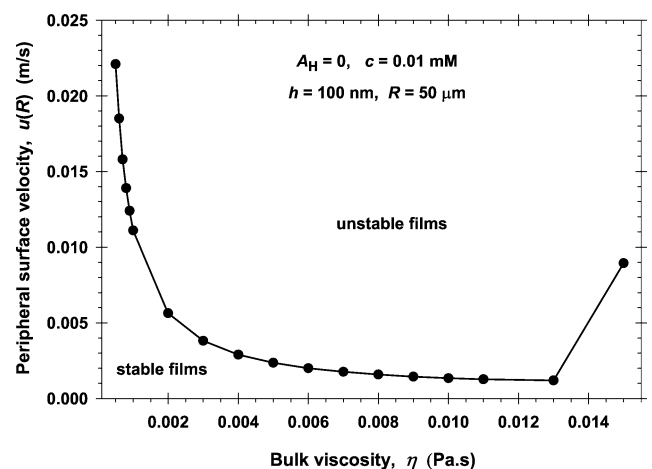


Fig. 8. Stability–instability diagram, $u(R)$ vs η , calculated for $A_H = 0$, $c = 0.01 \text{ mM}$, $h = 100 \text{ nm}$, and $R = 50 \mu\text{m}$. The curve represents the boundary between the regions of stable and unstable films.

dence, in Fig. 8 we present a stability diagram in coordinates $u(R)$ vs η . In this case, the boundary between the regions of stability and instability is nonmonotonic: at lower η the stability decreases with the rise of viscosity, whereas the opposite trend is observed at higher η . This could be attributed to the competition of two effects: (i) the increase of η promotes the transfer of momentum from the moving adsorption layers at the film surfaces to the film interior, which enhances the development of instability; (ii) at sufficiently high η the viscous dissipation damps the hydrodynamic flows and, consequently, hinders the mutual approach of the two film surfaces.

Last but not least, the transition from stable to unstable film is affected also by the bulk surfactant concentration, c ; see Fig. 9. The increase of c leads to an increase of Γ_e and E_G , to a decrease of σ and h_a , and to variations of b and h_s , see Eqs. (3), (25), and (27). The interplay of all aforementioned effects leads to a relatively simple result: the stability increases with the rise of surfactant concentration (Fig. 9).

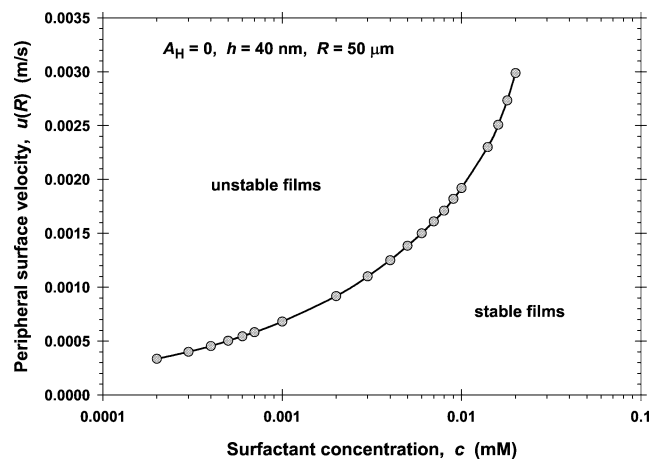


Fig. 9. Stability–instability diagram, $u(R)$ vs c , calculated for $A_H = 0$, $h = 40$ nm, $R = 50$ μm , and $\eta = 1$ mPa s. The curve represents the boundary between the regions of stable and unstable films.

One possible explanation stems from Fig. 4b, which indicates that the difference, $2\delta\Gamma(0)$, between the adsorptions at the front and rear drop surface, decreases with the rise of c . This decrease in the concentration polarization leads to a deceleration in the diffusion transfer of surfactant across the film, and to a suppression of the diffusion-driven instabilities.

6.3. Mechanism of film destabilization

To investigate how the diffusion-driven instability develops, we applied a computer modeling based on numerical integration of Eqs. (59) and (60). Because our aim is to demonstrate the effect of the bulk and surface diffusion, in the computations we set the disjoining pressure equal to zero, that is $A_H = 0$. To specify the state of the system, we chose the point corresponding to $\delta\Gamma(R)/\Gamma_e = 0.003$ in Fig. 5a. For diffusivity values $D = D_s = 2.6, 2.8$, and 3.0×10^{-6} cm^2/s (all other parameters being the same as for the continuous curve in Fig. 5a) we calculated the transitional thickness to be, respectively, $h_{tr} = 61.5, 62.9$, and 64.3 nm.

To find the shape of the perturbed film surfaces, we consider an axisymmetric perturbation, described by the functions $\bar{h}(x)$ and $\bar{p}(x)$; see Eqs. (59)–(61). Equations (59) and (60) are integrated numerically using the boundary conditions

$$\begin{aligned} \bar{h}(0) = -\varepsilon, \quad \left. \frac{\partial \bar{h}}{\partial x} \right|_{x=0} = \left. \frac{\partial \bar{p}}{\partial x} \right|_{x=0} = 0, \\ \bar{h}(1) = \bar{p}(1) = 0, \end{aligned} \quad (76)$$

where, as before, $x = 0$ and $x = 1$ denote the film center and periphery, respectively. One sees, that the perturbation is specified by a given small value, $\bar{h}(0) = -\varepsilon$, of the change in thickness at the film center. Indeed, all other boundary conditions in Eq. (76) are trivial. Results of the integration are shown in Fig. 10.

Figures 10a and 10b present the calculated axisymmetric perturbations $\bar{h}(x)$ and $\bar{p}(x)$ for the case $h = 50$ nm $< h_{tr}$,

corresponding to the domain of unstable films (Fig. 5a). One sees that the small decrease in the the film thickness at the film center, $\bar{h}(0)/\varepsilon = -1$, leads to the appearance of a well pronounced local minimum of depth $\bar{h}(0.62)/\varepsilon \approx -4$ for $D = 3 \times 10^{-10}$ m^2/s in Fig. 10a. In other words, an occasional concavity, $\bar{h}(0) = -\varepsilon$, is spontaneously amplified by the unstable system (for which $h < h_{tr}$).

In contrast, Fig. 10c shows that there is no such amplification of the perturbation $\bar{h}(0)/\varepsilon = -1$ when the system is stable: for $h = 70$ nm $> h_{tr}$. In the latter case, the perturbational thickness $\bar{h}(x)/\varepsilon$ decays monotonically from -1 to 0, and a development of a local minimum in thickness at $0 < x < 1$ (like that in Fig. 10a) is not observed. Moreover, the magnitude of the fluctuational pressure, $\bar{p}(x)$, is negligibly small in Fig. 10d as compared to Fig. 10b.

It should be also noted that the depth of the local minima in Figs. 10a and 10b increases with the rise of the diffusion coefficients D and D_s . Moreover, the “dimple-like” shape of the perturbed film profile (Fig. 10a) is nontrivial: the film thickness is minimal somewhere in the interior of the interval $0 < x < 1$, rather than at the film center, where the thickness turns out to be maximal. This shape of the perturbed film surfaces is accompanied by a corresponding variation in the perturbational pressure, $\bar{p}(x)$, which exhibits a local depression in the vicinity of the region where the perturbed film has its minimal thickness, see Figs. 10a and 10b. We recall that in the nonperturbed film, the pressure is uniform, $\partial p/\partial r = 0$, see Eq. (18).

The calculated curves in Fig. 10 can be interpreted in the following way. If occasionally a local perturbational decrease of the thickness with $\bar{h}(0) = -\varepsilon$ happens at the central part of the film, it leads to an acceleration of the surfactant diffusion across the film and of the related surfactant transport along the film surfaces (Fig. 1b). The latter, in its own turn, accelerates the circulation of the fluid inside the film (Fig. 3) and gives rise to a local lowering of the pressure somewhere in the interior of the region $0 < x < 1$. For $h < h_{tr}$ the system amplifies the perturbation, the surfactant-driven fluid circulation causes a considerable local minimum of the pressure (Fig. 10b), that forces the film surfaces to bend in (Fig. 10a), and eventually to touch each other, which would lead to film rupturing. In contrast, for $h > h_{tr}$ the system does not amplify the perturbation and the film remains stable: see Fig. 10c where $|\bar{h}(x)/\varepsilon| \leq 1$, and Fig. 10d where the perturbational pressure is relatively small.

Thus, the major reason for film breakage is the surfactant diffusion across the film, engendered by the different adsorptions at the two film surfaces, which causes the circulation of the liquid inside the film, and leads to the development of an instability when the film thickness is sufficiently small.

Note that the above mechanism of film breakage is essentially different from that proposed by Vries [56] and developed in subsequent studies [48,49,57–59], where the instability is due to the action of an attractive disjoining pressure, $\Pi(h)$. The latter mechanism provides a simple criterion for rupturing of an axisymmetric film of radius R ; see,

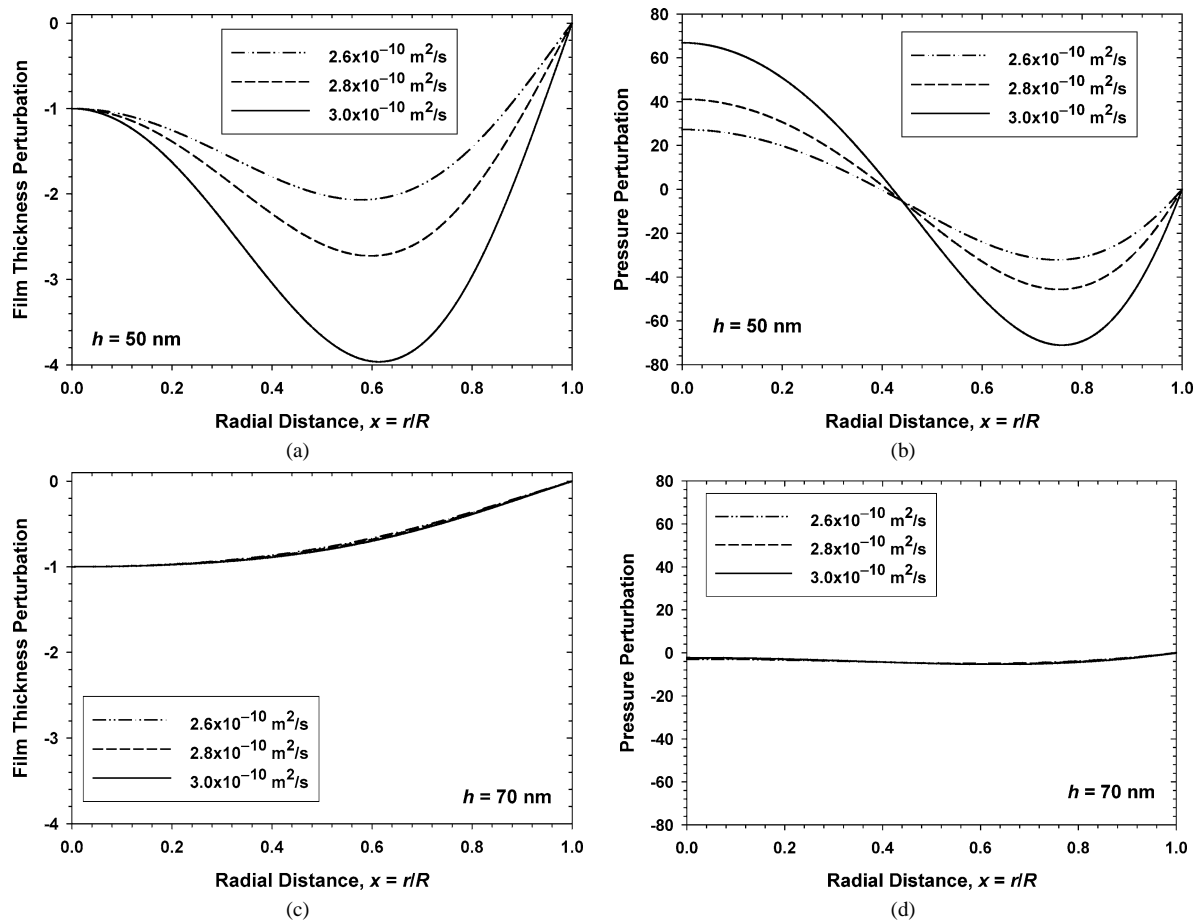


Fig. 10. Dimensionless axisymmetric perturbations in film thickness, $\bar{h}(x)/\varepsilon$, and pressure, $\bar{p}(x)$, calculated by solving numerically Eqs. (59)–(60), along with the boundary conditions, Eq. (76); \bar{h} is scaled with h , and \bar{p} —with $\sigma h/(2R^2)$, see Eq. (61). Plots of (a) $\bar{h}(x)/\varepsilon$ and (b) $\bar{p}(x)$ for $h = 50 \text{ nm} < h_{tr}$, corresponding to *unstable* films. Plots of (c) $\bar{h}(x)/\varepsilon$ and (d) $\bar{p}(x)$ for $h = 70 \text{ nm} > h_{tr}$, corresponding to *stable* films; see the text for details.

e.g., Ref. [55],

$$\frac{2R^2}{\sigma} \left(\frac{\partial \Pi}{\partial h} \right) \geq j_1^2 \approx 5.783, \quad (77)$$

where j_1 is the first zero of the Bessel function J_0 . However, if a sufficiently strong repulsive force is present (say a double-layer or steric-overlap repulsion), it can counterbalance the van der Waals attraction and the film can reach an equilibrium state. In such a case, the derivative $\partial \Pi / \partial h$ is negative, the criterion, Eq. (77), is not satisfied, and the films should be stable. The latter prediction of the de Vries model contradicts to the experiment, insofar as liquid films, in which electrostatic or steric forces are operative (films stabilized by ionic or nonionic surfactants) also exhibit instabilities and rupture. Note that the diffusion-driven instability, investigated in the present paper, can lead to film breakage irrespective of whether the derivative $\partial \Pi / \partial h$ is positive, negative or zero; see Figs. 5 and 10.

7. Summary and concluding remarks

When an emulsion drop or gas bubble is moving through a narrow capillary (Fig. 1a), the viscous friction in the liq-

uid film, intervening between the drop/bubble and the inner capillary wall, influences the surface density, Γ , of the adsorbed surfactant molecules. Γ increases at the rear part of the front drop, but decreases at the front part of the rear drop, see Fig. 1b and Eq. (6). This “polarization” in the surface concentrations gives rise to a diffusion transfer of surfactant molecules across the liquid film separating the two neighboring drops (bubbles). Solving the respective hydrodynamic problem, we derived expressions describing the variations of adsorption and velocity along the drop surfaces in the zone of their contact: see Eqs. (22), (26), and (29), and Figs. 3 and 4.

The diffusion of surfactant across the film between two ganglia (drops, bubbles) may promote its destabilization and rupturing, which is equivalent to coalescence of the two ganglia. To analyze the conditions for such destabilization, we applied a linear stability analysis (Section 4). Small perturbations in all physical parameters were introduced and the full set of equations is linearized. After some transformations, the problem was reduced to a set of six equations, Eqs. (48) and (53)–(57). Further transformations lead to a system of two differential equations, Eqs. (59) and (60). The solution of the latter system depends on three integra-

tion constants, H_0 , H_1 , and H_2 which are determined from a linear homogeneous system of equations, Eq. (72). Equation (74), which expresses the condition for existence of a nontrivial solution to the perturbation problem, represents a criterion for transition from stable to unstable films. This criterion implies that the boundary between the regions of stability and instability depends on a number of parameters, whose influence have been investigated.

The computations (Figs. 5–9) show that the increase of the thickness, h , between two neighboring bubbles (or drops) and of the surfactant concentration, c , have a stabilizing effect, whereas the increase of the film radius, R , and surface velocity, u , lead to destabilization. The effect of the colloidal surface forces, characterized by the Hamaker constant, was found to be insignificant for the stability–instability transition (Fig. 5). The diffusion mechanism for film rupturing, described in this paper, may lead to breakage of liquid films of thickness > 200 nm (Fig. 6), for which the effect of the surface forces is negligible. The film rupturing occurs through a dimple-like perturbation in the film thickness (Fig. 10a), which is due to a local lowering in the pressure (Fig. 10b) caused by a faster circulation of the liquid inside the film (Fig. 3), which in its own turn is engendered by the accelerated surfactant diffusion across the thinner parts of the film.

It should be noted that the above hydrodynamic mechanism involves many dimensionless groups of parameters, so it is practically impossible to specify a single dimensionless group providing a simple criterion about whether or not this mode of instability will occur for a given system. For this reason, we have specified the surfactant (Triton X-100), for which the computations have been carried out. Likewise, for another given system, the occurrence of such a diffusion-driven instability can be predicted numerically, by computation of a stability–instability diagram, like one of those in Figs. 5–9.

Acknowledgment

This study was supported by the Inco-Copernicus Project, No. IC15CT980911, of the European Commission.

Appendix A. Surfactant distribution across the film

We consider a liquid film of thickness, h , which is stabilized by a surfactant that is soluble only in the phase of the film. The adsorption at the left film surface ($z = 0$) is Γ_2 and at the right film surface ($z = h$) it is Γ_1 ; see Fig. 1b. The difference between the adsorptions at the two film surfaces gives rise to a diffusion across the film, where the surfactant concentration, c , obeys the equation

$$\frac{\partial c}{\partial t} = D \frac{\partial^2 c}{\partial z^2}. \tag{A.1}$$

D is the diffusivity of the surfactant molecules. The boundary conditions at the two film surfaces are

$$\frac{\partial \Gamma_2}{\partial t} = D \frac{\partial c}{\partial z} \quad \text{at } z = 0, \tag{A.2}$$

$$\frac{\partial \Gamma_1}{\partial t} = -D \frac{\partial c}{\partial z} \quad \text{at } z = h. \tag{A.3}$$

For small perturbations, the relation between the adsorption and subsurface concentration are given by the linearized adsorption isotherm

$$\Gamma_2 = h_a c|_{z=0} \quad \text{and} \quad \Gamma_1 = h_a c|_{z=h}, \tag{A.4}$$

where $h_a = (\partial \Gamma / \partial c)_e$. We seek $c(z, t)$ in the form

$$c = \sum_k B_k \exp(-\lambda_k^2 D t) [-\lambda_k h_a \sin(\lambda_k z) + \cos(\lambda_k z)], \tag{A.5}$$

which satisfies the boundary condition, Eq. (A.2). Substituting Eq. (A.5) into the other boundary condition, Eq. (A.3), we determine the eigenvalues λ_k , which are given by the roots of the characteristic equation

$$\tan(\lambda_k h) = \frac{2\lambda_k h_a}{(\lambda_k h_a)^2 - 1}. \tag{A.6}$$

The slowest relaxation of the surfactant concentration $c(z, t)$ corresponds to the lowest eigenvalue, λ_1 . If $h_a/h \ll 1$, from Eq. (A.6) we get $\lambda_1^2 = 2/(h h_a)$. Substituting the latter value into Eq. (A.5) we obtain

$$c \propto \exp\left(-\frac{2Dt}{h h_a}\right) (2z/h - 1). \tag{A.7}$$

Equation (A.7) shows that the surfactant concentration is a linear function of z , and decays exponentially with the time, t .

In Eq. (13) we assumed that the deviations from equilibrium at the two surfaces of the film between two bubbles (or drops, Fig. 1b) are *antisymmetric*. Here we will confirm that this is really the case. We start with a more general form of Eq. (13), viz.,

$$\Gamma_1 = \Gamma_e + \delta \Gamma_1(r), \quad \Gamma_2 = \Gamma_e + \delta \Gamma_2(r). \tag{A.8}$$

Our aim is to prove that $\delta \Gamma_1 = -\delta \Gamma_2$. With this end in view, we consider small deviations from equilibrium which are, in general, different at the two film surfaces, and will be denoted by subscripts 1 and 2. For such a small deviation, using the lubrication approximation, from the basic equations (7), (8), (12), (15), (16), (20), and (21), one can derive the following relationships:

$$\frac{\partial p}{\partial r} = \frac{1}{h} \frac{\partial \sigma}{\partial \Gamma} \frac{\partial}{\partial r} (\delta \Gamma_1 + \delta \Gamma_2), \tag{A.9}$$

$$\begin{aligned} & \Gamma_e (u_1 + u_2) + \frac{h}{2} c_e (u_1 + u_2) \\ & - \frac{h^3 c_e}{12 \eta} \frac{\partial p}{\partial r} - \frac{D h}{2 h_a} \frac{\partial}{\partial r} (\delta \Gamma_1 + \delta \Gamma_2) \\ & - D_s \frac{\partial}{\partial r} (\delta \Gamma_1 + \delta \Gamma_2) = 0. \end{aligned} \tag{A.10}$$

Eliminating $\partial p/\partial r$ between Eqs. (A.9) and (11), we get

$$u_1 + u_2 = \frac{h}{6\eta} \frac{\partial \sigma}{\partial \Gamma} \frac{\partial}{\partial r} (\delta\Gamma_1 + \delta\Gamma_2). \quad (\text{A.11})$$

Furthermore, we substitute $u_1 + u_2$ from Eq. (A.11) into the first two terms of Eq. (A.10). The result reads

$$\left(\frac{Dh}{2h_a} + D_s + \frac{hE_G}{6\eta} \right) \frac{\partial}{\partial r} (\delta\Gamma_1 + \delta\Gamma_2) = 0. \quad (\text{A.12})$$

Equation (A.12) implies $\delta\Gamma_1 = -\delta\Gamma_2$, which confirms the validity of the expressions for Γ_1 and Γ_2 in Eq. (13).

Appendix B. Relationships between the perturbations of the physical parameters

Our aim here is to derive Eqs. (53)–(57). Substituting the perturbations, defined by Eqs. (31)–(33), into the Navier–Stokes and continuity equations, (7) and (8), we obtain

$$\frac{\partial \tilde{p}}{\partial r} = \eta \frac{\partial^2 \tilde{v}_r}{\partial z^2}, \quad (\text{B.1})$$

$$\frac{1}{r} \frac{\partial}{\partial r} (r \tilde{v}_r) + \frac{\partial \tilde{v}_z}{\partial z} = 0. \quad (\text{B.2})$$

Next, we integrate Eq. (B.1) twice with respect to z and use the boundary conditions, Eqs. (38) and (39); thus we get

$$\begin{aligned} \tilde{v}_r = & \frac{z(z-h)}{2\eta} \frac{\partial \tilde{p}}{\partial r} + \frac{z}{h} \left(\frac{2u}{h} \tilde{h}_1 + \tilde{u}_1 \right) \\ & + \frac{h-z}{h} \left(\frac{2u}{h} \tilde{h}_2 + \tilde{u}_2 \right). \end{aligned} \quad (\text{B.3})$$

To determine \tilde{v}_z we substitute Eq. (B.3) into Eq. (B.2), integrate with respect to z , and use the boundary condition, Eq. (43); the result reads

$$\begin{aligned} \tilde{v}_z = & \frac{\partial \tilde{h}_2}{\partial t} - \frac{1}{r} \frac{\partial}{\partial r} \left\{ r \left[\frac{z^2(2z-3h)}{12\eta} \frac{\partial \tilde{p}}{\partial r} - u \tilde{h}_2 \right. \right. \\ & \left. \left. + \frac{z^2}{2h} \left(\tilde{u}_1 + \frac{2u}{h} \tilde{h}_1 \right) + \frac{z(2h-z)}{2h} \left(\tilde{u}_2 + \frac{2u}{h} \tilde{h}_2 \right) \right] \right\}. \end{aligned} \quad (\text{B.4})$$

Substituting $z = h$ in Eq. (B.4), and employing Eqs. (42) and (49), we obtain

$$\frac{\partial \tilde{h}}{\partial t} = \frac{1}{r} \frac{\partial}{\partial r} \left[r \left(\frac{h^3}{12\eta} \frac{\partial \tilde{p}}{\partial r} - h \frac{\tilde{u}_1 + \tilde{u}_2}{2} \right) \right]. \quad (\text{B.5})$$

In the transitional regime we apply Eq. (52), and from Eq. (B.5) deduce Eq. (53); we have used that the expression in the parentheses in Eq. (B.5) must be regular for $r \rightarrow 0$.

Further, we introduce perturbations in the surface stress balance, Eq. (20):

$$\begin{aligned} -\frac{E_G}{\Gamma_e} \frac{\partial \Gamma_1}{\partial r} - \frac{E_G}{\Gamma_e} \frac{\partial \tilde{\Gamma}_1}{\partial r} = & \eta \frac{\partial v_r}{\partial z} \Big|_{z=h+\tilde{h}_1} \\ = & \eta \frac{\partial v_r}{\partial z} \Big|_{z=h} + \eta \frac{\partial^2 v_r}{\partial z^2} \Big|_{z=h} \tilde{h}_1 + \eta \frac{\partial \tilde{v}_r}{\partial z} \Big|_{z=h}. \end{aligned} \quad (\text{B.6})$$

Equation (19) implies that $\partial^2 v_r / \partial z^2 = 0$. Utilizing again Eq. (20), from Eq. (B.6) we derive

$$\eta \frac{\partial \tilde{v}_r}{\partial z} \Big|_{z=h} = -\frac{E_G}{\Gamma_e} \frac{\partial \tilde{\Gamma}_1}{\partial r}. \quad (\text{B.7})$$

Likewise, from Eq. (21) we deduce

$$\eta \frac{\partial \tilde{v}_r}{\partial z} \Big|_{z=0} = \frac{E_G}{\Gamma_e} \frac{\partial \tilde{\Gamma}_2}{\partial r}. \quad (\text{B.8})$$

The differentiation of Eq. (B.3) yields

$$\eta \frac{\partial \tilde{v}_r}{\partial z} = \left(z - \frac{h}{2} \right) \frac{\partial \tilde{p}}{\partial r} + \frac{\eta}{h} \left(\frac{u}{h} \tilde{h} + \tilde{u}_1 \right) - \frac{\eta}{h} \left(-\frac{u}{h} \tilde{h} + \tilde{u}_2 \right). \quad (\text{B.9})$$

Next, in Eq. (B.9) we set $z = h$ and $z = 0$ and apply Eqs. (B.7) and (B.8):

$$\frac{h}{2} \frac{\partial \tilde{p}}{\partial r} + \frac{\eta}{h} \left(\frac{2u}{h} \tilde{h} + \tilde{u}_1 - \tilde{u}_2 \right) = -\frac{E_G}{\Gamma_e} \frac{\partial \tilde{\Gamma}_1}{\partial r}, \quad (\text{B.10})$$

$$-\frac{h}{2} \frac{\partial \tilde{p}}{\partial r} + \frac{\eta}{h} \left(\frac{2u}{h} \tilde{h} + \tilde{u}_1 - \tilde{u}_2 \right) = \frac{E_G}{\Gamma_e} \frac{\partial \tilde{\Gamma}_2}{\partial r}. \quad (\text{B.11})$$

Taking the sum and the difference of Eqs. (B.10) and (B.11) we derive Eqs. (54) and (55).

To derive Eqs. (56) and (57), we first apply the lubrication approximation ($h/R \ll 1$) in the diffusion equation (50):

$$\frac{\partial \tilde{c}}{\partial t} + \tilde{v}_z \frac{\partial \tilde{c}}{\partial z} = D \frac{\partial^2 \tilde{c}}{\partial z^2}. \quad (\text{B.12})$$

With the help of Eq. (14), in the steady state limit ($t \gg h^2/D$) we bring Eq. (B.12) in the form

$$2 \frac{\delta c_s}{h} \tilde{v}_z = D \frac{\partial^2 \tilde{c}}{\partial z^2}, \quad (\text{B.13})$$

where we have used the relationship $\delta\Gamma/h_a = \delta c_s$. Next, we introduce perturbations in the boundary conditions, Eqs. (15) and (16). Taking into account that $\partial^2 c / \partial z^2 = 0$ (see Eq. (12)), we derive

$$\frac{\partial \tilde{\Gamma}_1}{\partial t} + \frac{1}{r} \frac{\partial}{\partial r} \left[r \left(-\tilde{\Gamma}_1 u + \Gamma_e \tilde{u}_1 - D_s \frac{\partial \tilde{\Gamma}_1}{\partial r} \right) \right] = -D \frac{\partial \tilde{c}}{\partial z} \Big|_{z=h}, \quad (\text{B.14})$$

$$\frac{\partial \tilde{\Gamma}_2}{\partial t} + \frac{1}{r} \frac{\partial}{\partial r} \left[r \left(\tilde{\Gamma}_2 u + \Gamma_e \tilde{u}_2 - D_s \frac{\partial \tilde{\Gamma}_2}{\partial r} \right) \right] = D \frac{\partial \tilde{c}}{\partial z} \Big|_{z=0}. \quad (\text{B.15})$$

Summing up the latter two equations, we get

$$\begin{aligned} \frac{\partial}{\partial t} (\tilde{\Gamma}_1 + \tilde{\Gamma}_2) + \frac{1}{r} \frac{\partial}{\partial r} \left\{ r \left[u (\tilde{\Gamma}_2 - \tilde{\Gamma}_1) + \Gamma_e (\tilde{u}_1 + \tilde{u}_2) \right. \right. \\ \left. \left. - D_s \frac{\partial}{\partial r} (\tilde{\Gamma}_1 + \tilde{\Gamma}_2) \right] \right\} = -D \int_0^h \frac{\partial^2 \tilde{c}}{\partial z^2} dz. \end{aligned} \quad (\text{B.16})$$

To estimate the right-hand side of Eq. (B.16), we employ Eq. (B.13):

$$D \int_0^h \frac{\partial^2 \tilde{c}}{\partial z^2} dz = 2 \frac{\delta c_s}{h} \int_0^h \tilde{v}_z dz. \quad (\text{B.17})$$

In Eq. (B.17) we substitute \tilde{v}_z from Eq. (B.4), integrate, and substitute the expression for $\partial \tilde{h}_2 / \partial t = -(\partial \tilde{h} / \partial t) / 2$ from Eq. (B.5). After some transformations, we obtain

$$D \int_0^h \frac{\partial^2 \tilde{c}}{\partial z^2} dz = -\frac{\delta c_s}{r} \frac{\partial}{\partial r} \left\{ r \left[\frac{h}{6} (\tilde{u}_2 - \tilde{u}_1) + \frac{2u}{3} \tilde{h} \right] \right\}. \quad (\text{B.18})$$

The term proportional to $\delta c_s u \tilde{h}$ is of the third order of magnitude and it is negligible. Moreover, having in mind that $\delta c_s = \delta \Gamma / h_a$ and $h / h_a \ll 1$ (see Appendix A), we get

$$\Gamma_e (\tilde{u}_1 + \tilde{u}_2) \gg \frac{h \delta \Gamma}{6 h_a} (\tilde{u}_2 - \tilde{u}_1). \quad (\text{B.19})$$

Hence, in view of Eq. (B.18), we may conclude that the right-hand side of Eq. (B.16) is of a higher order of magnitude and can be neglected. Then, imposing the condition for transitional regime, Eq. (52), from Eq. (B.16) we deduce Eq. (56).

Furthermore, we introduce small perturbations into the relation, Eq. (A.4), between the subsurface concentration of surfactant and its adsorption:

$$c|_{z=\tilde{h}_2} = c|_{z=0} + \tilde{c}|_{z=0} + \frac{\partial c}{\partial z} \Big|_{z=0} \tilde{h}_2 = \frac{\Gamma_2}{h_a} + \frac{\tilde{\Gamma}_2}{h_a}. \quad (\text{B.20})$$

With the help of Eq. (14), from Eq. (B.20) we derive

$$\tilde{c}|_{z=0} = \frac{\tilde{\Gamma}_2}{h_a} + \frac{\delta c_s}{h} \tilde{h}. \quad (\text{B.21})$$

Likewise, for the other film surface we get

$$\tilde{c}|_{z=h} = \frac{\tilde{\Gamma}_1}{h_a} - \frac{\delta c_s}{h} \tilde{h}. \quad (\text{B.22})$$

Further, our aim is to estimate the right-hand side of Eq. (B.15). With this end in view, we integrate twice Eq. (B.13) with respect to z and obtain an expression for \tilde{c} ,

$$\tilde{c} = \frac{2 \delta c_s}{Dh} \int_0^z dz_1 \int_0^{z_1} dz_2 \tilde{v}_z + A_1 z + A_2, \quad (\text{B.23})$$

where z_1 and z_2 are integration variables, while A_1 and A_2 are constants of integration. At the next step, we first determine A_1 and A_2 from the boundary conditions, Eqs. (B.21) and (B.22), and then differentiate to derive

$$D \frac{\partial \tilde{c}}{\partial z} \Big|_{z=0} = -2 \frac{\delta c_s}{h^2} \int_0^h dz_1 \int_0^{z_1} dz_2 \tilde{v}_z + \frac{D}{h} \left(\frac{\tilde{\Gamma}_1}{h_a} - \frac{\delta c_s}{h} \tilde{h} \right) - \frac{D}{h} \left(\frac{\tilde{\Gamma}_2}{h_a} + \frac{\delta c_s}{h} \tilde{h} \right). \quad (\text{B.24})$$

In Eq. (B.24) we substitute \tilde{v}_z from Eq. (B.4), carry out the integration, and finally substitute the expression for $\partial \tilde{h}_2 / \partial t = -(\partial \tilde{h} / \partial t) / 2$ from Eq. (B.5). The result reads

$$D \frac{\partial \tilde{c}}{\partial z} \Big|_{z=0} = \frac{D}{h} \left(\frac{\tilde{\Gamma}_1 - \tilde{\Gamma}_2}{h_a} - 2 \frac{\delta c_s}{h} \tilde{h} \right) + \frac{\delta c_s}{r} \frac{\partial}{\partial r} \left[r \left(\frac{u \tilde{h}}{3} + \frac{h^3}{60 \eta} \frac{\partial \tilde{p}}{\partial r} - \frac{h \tilde{u}_1}{6} \right) \right]. \quad (\text{B.25})$$

Then, Eq. (B.25) is substituted into the right-hand side of Eq. (B.15):

$$\begin{aligned} \frac{\partial \tilde{\Gamma}_2}{\partial t} - \frac{D}{h} \left(\frac{\tilde{\Gamma}_1 - \tilde{\Gamma}_2}{h_a} - 2 \frac{\delta c_s}{h} \tilde{h} \right) &+ \frac{1}{r} \frac{\partial}{\partial r} \left[r \left(\tilde{\Gamma}_2 u + \Gamma_e \tilde{u}_2 - D_s \frac{\partial \tilde{\Gamma}_2}{\partial r} \right) \right] \\ &= \frac{\delta c_s}{2r} \frac{\partial}{\partial r} \left[r \left(\frac{2u}{3} \tilde{h} + \frac{h^3}{30 \eta} \frac{\partial \tilde{p}}{\partial r} - \frac{h}{3} \tilde{u}_1 \right) \right]. \end{aligned} \quad (\text{B.26})$$

Next, we substitute the derivative, $\partial \tilde{p} / \partial r$, from Eq. (B.5) in (B.26); the result can be expressed in the form

$$\begin{aligned} \frac{\partial}{\partial t} \left(\tilde{\Gamma}_2 - \frac{\delta c_s}{5} \tilde{h} \right) - \frac{D}{h} \left(\frac{\tilde{\Gamma}_1 - \tilde{\Gamma}_2}{h_a} - 2 \frac{\delta c_s}{h} \tilde{h} \right) &+ \frac{1}{r} \frac{\partial}{\partial r} \left[r \left(\tilde{\Gamma}_2 u + \Gamma_e \tilde{u}_2 - D_s \frac{\partial \tilde{\Gamma}_2}{\partial r} \right) \right] \\ &= \frac{\delta c_s}{r} \frac{\partial}{\partial r} \left[r \left(\frac{u}{3} \tilde{h} - \frac{4h}{15} \tilde{u}_1 - \frac{h}{10} \tilde{u}_2 \right) \right]. \end{aligned} \quad (\text{B.27})$$

Using again estimates related to Eq. (B.19), we establish that the right-hand side of Eq. (B.27) is negligible. Finally, imposing the condition for transitional regime, Eq. (52), from Eq. (B.27) we obtain Eq. (57), where we have substituted $\delta c_s = \delta \Gamma / h_a$.

Appendix C. Final set of equations and boundary conditions

Our purpose is to derive Eqs. (59) and (60) starting from Eqs. (48) and (53)–(57). With this end in view, in Eq. (56) we substitute $\tilde{u}_1 + \tilde{u}_2$ from Eq. (53) and $\tilde{\Gamma}_1 + \tilde{\Gamma}_2$ from Eq. (54). As a result, we bring Eq. (56) into the form

$$\tilde{\Gamma}_2 - \tilde{\Gamma}_1 = -\frac{h^2 \Gamma_e}{6 \eta} \left(1 + \frac{h_s}{h} \right) \left(\frac{1}{u} \frac{\partial \tilde{p}}{\partial r} \right), \quad (\text{C.1})$$

where, as before, $h_s = 6 \eta D_s / E_G$. Next, we eliminate $\tilde{\Gamma}_1$ between Eqs. (54) and (C.1), and get

$$u \tilde{\Gamma}_2 = -\frac{h \Gamma_e}{2 E_G} u \tilde{p} - \frac{h^2 \Gamma_e}{12 \eta} \left(1 + \frac{h_s}{h} \right) \frac{\partial \tilde{p}}{\partial r}. \quad (\text{C.2})$$

Likewise, we eliminate \tilde{u}_1 between Eqs. (53) and (55), and obtain

$$\tilde{u}_2 \Gamma_e = \frac{h^2 \Gamma_e}{12 \eta} \frac{\partial \tilde{p}}{\partial r} - \frac{E_G h}{4 \eta} \frac{\partial}{\partial r} (\tilde{\Gamma}_2 - \tilde{\Gamma}_1) + \frac{\Gamma_e}{h} u \tilde{h}. \quad (\text{C.3})$$

Next, we divide Eq. (C.2) by u and differentiate; the result can be expressed in the form

$$-D_s \frac{\partial \tilde{\Gamma}_2}{\partial r} = \frac{h\Gamma_e D_s}{2E_G} \frac{\partial \tilde{p}}{\partial r} + \frac{h^2 \Gamma_e D_s}{12\eta} \left(1 + \frac{h_s}{h}\right) \frac{\partial}{\partial r} \left(\frac{1}{u} \frac{\partial \tilde{p}}{\partial r}\right). \quad (\text{C.4})$$

We sum up Eqs. (C.2), (C.3), and (C.4), and substitute the result into Eq. (57), where we further express $\tilde{\Gamma}_2 - \tilde{\Gamma}_1$ using Eq. (C.1). Thus, we obtain an equation containing only two unknown functions, \tilde{h} and \tilde{p} :

$$\begin{aligned} \frac{1}{r} \frac{\partial}{\partial r} \left\{ r \left[\frac{E_G h^3 \Gamma_e}{72\eta^2} \left(1 + \frac{h_s}{h}\right) \left(3 + \frac{h_s}{h}\right) \frac{\partial}{\partial r} \left(\frac{1}{u} \frac{\partial \tilde{p}}{\partial r}\right) \right. \right. \\ \left. \left. + \frac{\Gamma_e}{h} u \tilde{h} - \frac{h\Gamma_e}{2E_G} u \tilde{p} \right] \right\} \\ = \frac{Dh\Gamma_e}{6h_a\eta} \left(1 + \frac{h_s}{h}\right) \left(\frac{1}{u} \frac{\partial \tilde{p}}{\partial r}\right) - \frac{2D}{h_a h^2} \tilde{h} \delta\Gamma. \end{aligned} \quad (\text{C.5})$$

Equations (48) and (C.5) form a set of two equations for determining \tilde{h} and \tilde{p} . Next, in Eqs. (48) and (C.5) we substitute $\delta\Gamma$ and u from Eq. (29), and II' from Eq. (58). Then, introducing the dimensionless variables defined by Eqs. (61) and (62), we transform Eqs. (48) and (C.5) into Eqs. (59) and (60).

Finally, we note that the differentiation of Eq. (54), in view of Eqs. (61) and (70), yields

$$(\partial \tilde{p} / \partial x)_{x=1} = 0, \quad (\text{C.6})$$

which is one of the relationships in Eq. (71). Likewise, the differentiation of Eq. (C.1), in view of Eqs. (29), (61), and (70), gives

$$\left[\frac{\partial}{\partial x} \left(\frac{1}{x} \frac{\partial \tilde{p}}{\partial x} \right) \right]_{x=1} = 0. \quad (\text{C.7})$$

Combining Eqs. (C.6) and (C.7), we get $(\partial^2 \tilde{p} / \partial x^2)_{x=1} = 0$, which is also used in Eq. (71).

References

- [1] A.C. Payatakes, M.M. Dias, *Rev. Chem. Eng.* 2 (1984) 85.
- [2] D.D. Huang, A.D. Nikolov, D.T. Wasan, *Langmuir* 2 (1986) 672.
- [3] W.R. Rossen, P.A. Gauglitz, *AIChE J.* 36 (1990) 1176.
- [4] G. Singh, G.J. Hirasaki, C.A. Miller, *AIChE J.* 43 (1997) 3241.
- [5] R. Szafranski, J.B. Lawson, G.J. Hirasaki, C.A. Miller, N. Akiya, S. King, R.E. Jackson, H. Meinardus, J. Londergan, *Prog. Colloid Polym. Sci.* 111 (1998) 162.
- [6] K. Suzuki, I. Shuto, Y. Hagura, *Food Sci. Technol. Int.* 2 (1996) 43.
- [7] S.M. Joscelyne, G. Trägårdh, *J. Membr. Sci.* 169 (2000) 107.
- [8] P. Lipp, C.H. Lee, A.G. Fane, C.J.D. Fell, *J. Membr. Sci.* 36 (1988) 161.
- [9] M. Hlavacek, *J. Membr. Sci.* 102 (1995) 1.
- [10] I.W. Cumming, R.G. Holdich, I.D. Smith, *J. Membr. Sci.* 169 (2000) 147.
- [11] S.-H. Park, T. Yamaguchi, S. Nakao, *Chem. Eng. Sci.* 56 (2001) 3539.
- [12] J. Bullon, A. Cardenas, J. Sanchez, *J. Dispersion Sci. Technol.* 23 (2002) 269.
- [13] T.M. Tsai, M.J. Miksis, *J. Fluid Mech.* 274 (1994) 197.
- [14] G.N. Constantinides, A.C. Payatakes, *J. Colloid Interface Sci.* 141 (1991) 486.
- [15] G.N. Constantinides, A.C. Payatakes, *AIChE J.* 42 (1996) 369.
- [16] M.S. Valavanides, A.C. Payatakes, *Adv. Water Resources* 24 (2001) 385.
- [17] F. Fairbrother, A.E. Stubbs, *J. Chem. Soc.* 1 (1935) 527.
- [18] F.P. Bretherton, *J. Fluid Mech.* 10 (1961) 166.
- [19] C.-W. Park, G.M. Homsy, *J. Fluid Mech.* 139 (1984) 291.
- [20] G.J. Hirasaki, J.B. Lawson, *Soc. Pet. Eng. J.* 25 (1985) 176.
- [21] J.-D. Chen, *J. Colloid Interface Sci.* 109 (1986) 341.
- [22] L.W. Schwartz, H.M. Princen, A.D. Kiss, *J. Fluid Mech.* 172 (1986) 259.
- [23] J. Ratulowski, H.-C. Chang, *Phys. Fluids A* 1 (1989) 1642.
- [24] J. Ratulowski, H.-C. Chang, *J. Fluid Mech.* 210 (1990) 303.
- [25] M.J. Martinez, K.S. Udell, *J. Fluid Mech.* 210 (1990) 565.
- [26] C. Pozrikidis, *J. Fluid Mech.* 237 (1992) 627.
- [27] C. Quéguiner, D. Barthes-Bièsel, *J. Fluid Mech.* 348 (1997) 349.
- [28] C. Coulliette, C. Pozrikidis, *J. Fluid Mech.* 358 (1998) 1.
- [29] J.-L. Joye, G.J. Hirasaki, C.A. Miller, *Langmuir* 10 (1994) 3174.
- [30] D.A. Edwards, H. Brenner, D.T. Wasan, *Interfacial Transport Processes and Rheology*, Butterworth-Heinemann, Boston, 1991.
- [31] I.B. Ivanov, K.D. Danov, P.A. Kralchevsky, *Colloids Surf. A* 152 (1999) 161.
- [32] K.D. Danov, D.S. Valkovska, I.B. Ivanov, *J. Colloid Interface Sci.* 211 (1999) 291.
- [33] D.S. Valkovska, K.D. Danov, *J. Colloid Interface Sci.* 223 (2000) 314.
- [34] G.M. Ginley, C. Radke, *ACS Symp. Ser.* 369 (1989) 480.
- [35] C.-W. Park, *Phys. Fluids A* 4 (1992) 2335.
- [36] J. Chen, C. Zeev-Dagan, C. Maldarelli, *J. Fluid Mech.* 233 (1991) 405.
- [37] J. Chen, K.J. Stebe, *J. Fluid Mech.* 340 (1997) 35.
- [38] D.S. Valkovska, P.A. Kralchevsky, K.D. Danov, G. Broze, A. Mehreteab, *Langmuir* 16 (2000) 8892.
- [39] L.D. Landau, E.M. Lifshitz, *Fluid Mechanics*, Pergamon, Oxford, 1984.
- [40] I.B. Ivanov, D.S. Dimitrov, in: I.B. Ivanov (Ed.), *Thin Liquid Films*, Dekker, New York, 1988, p. 379.
- [41] I.B. Ivanov, *Pure Appl. Chem.* 52 (1980) 1241.
- [42] A. Bonfillon, D. Langevin, *Langmuir* 9 (1993) 2172.
- [43] I. Langmuir, *J. Am. Chem. Soc.* 15 (1918) 75.
- [44] C. Maldarelli, R.K. Jain, I.B. Ivanov, E. Ruckenstein, *J. Colloid Interface Sci.* 78 (1980) 118.
- [45] C. Maldarelli, R.K. Jain, in: I.B. Ivanov (Ed.), *Thin Liquid Films*, Dekker, New York, 1988, p. 497.
- [46] J.G.H. Joosten, in: I.B. Ivanov (Ed.), *Thin Liquid Films*, Dekker, New York, 1988, p. 569.
- [47] I.B. Ivanov, P.A. Kralchevsky, *Colloids Surf. A* 128 (1997) 155.
- [48] I.B. Ivanov, D.S. Dimitrov, *Colloid Polym. Sci.* 252 (1974) 982.
- [49] D.S. Valkovska, K.D. Danov, I.B. Ivanov, *Adv. Colloid Interface Sci.* 96 (2002) 101.
- [50] E.D. Manev, S.V. Sazdanova, D.T. Wasan, *J. Colloid Interface Sci.* 97 (1984) 591.
- [51] B.V. Derjaguin, *Theory of Stability of Colloids and Thin Liquid Films*, Plenum, New York, 1989.
- [52] J.N. Israelachvili, *Intermolecular and Surface Forces*, Academic Press, London, 1992.
- [53] P.A. Kralchevsky, K. Nagayama, *Particles at Fluid Interfaces and Membranes*, Elsevier, Amsterdam, 2001.
- [54] R.J. Gumerman, G.M. Homsy, *Chem. Eng. Commun.* 2 (1975) 27.
- [55] K.D. Danov, P.A. Kralchevsky, I.B. Ivanov, in: G. Broze (Ed.), *Handbook of Detergents, Part A: Properties*, Dekker, New York, 1999, p. 303.
- [56] A.J. Vries, *Rec. Trav. Chim. Pays-Bas* 77 (1958) 44.
- [57] A. Scheludko, *Proc. K. Akad. Wetensch. B* 65 (1962) 87.
- [58] A. Vrij, *Disc. Faraday Soc.* 42 (1966) 23.
- [59] I.B. Ivanov, B. Radoev, E. Manev, A. Scheludko, *Trans. Faraday Soc.* 66 (1970) 1262.